

Synthesis, Radiolabeling, and *In Vitro* and *In Vivo* Characterization of Heterobivalent Peptidic Agents for Bispecific EGFR and Integrin $\alpha_v\beta_3$ Targeting

Diana Braun,[†] Benedikt Judmann,[†] Xia Cheng, Björn Wängler, Ralf Schirmacher, Gert Fricker, and Carmen Wängler*



Cite This: *ACS Omega* 2023, 8, 2793–2807



Read Online

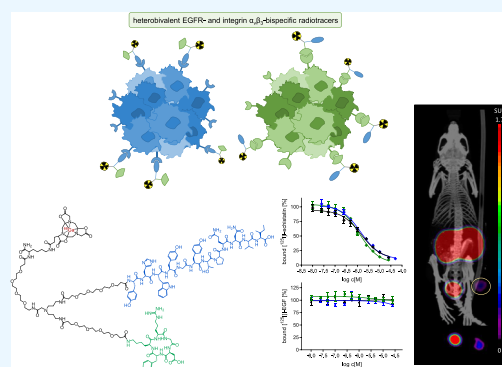
ACCESS |

Metrics & More

Article Recommendations

Supporting Information

ABSTRACT: Radiolabeled heterobivalent peptidic ligands (HBPLs) are a highly promising compound class for the sensitive and specific visualization of tumors as they often exhibit superior properties compared to their monospecific counterparts and are able to concomitantly or complementarily address different receptor types. The combination of two receptor-specific agents targeting the epidermal growth factor receptor (EGFR) and the integrin $\alpha_v\beta_3$ in one HBPL would constitute a synergistic combination of binding motifs as these two receptor types are concurrently overexpressed on several human tumor types and are closely associated with disease progression and metastasis. Here, we designed and synthesized two heterobivalent radioligands consisting of the EGFR-specific peptide GE11 and $\alpha_v\beta_3$ -specific cyclic RGD peptides, bearing a (1,4,7-triazacyclononane-4,7-diyl)diacetic acid-1-glutaric acid chelator for efficient radiolabeling and linkers of different lengths between both peptides. Both HBPLs were radiolabeled with $^{68}\text{Ga}^{3+}$ in high radiochemical yields, purities of 96–99%, and molar activities of 36–88 GBq/ μmol . [^{68}Ga]Ga-1 and [^{68}Ga]Ga-2 were evaluated for their $\log_{D(7.4)}$ and stability toward degradation by human serum peptidases, showing a high hydrophilicity for both agents of -3.07 ± 0.01 and -3.44 ± 0.08 as well as a high stability toward peptidase degradation in human serum with half-lives of 272 and 237 min, respectively. Further on, the *in vitro* receptor binding profiles of both HBPLs to the target EGF and integrin $\alpha_v\beta_3$ receptors were assessed on EGFR-positive A431 and $\alpha_v\beta_3$ -positive U87MG cells. Finally, we investigated the *in vivo* pharmacokinetics of HBPL [^{68}Ga]Ga-1 by positron emission tomography/computed tomography imaging in A431 tumor-bearing xenograft mice to assess its potential for the receptor-specific visualization of EGFR- and/or $\alpha_v\beta_3$ -expressing tumors. In these experiments, [^{68}Ga]Ga-1 demonstrated a tumor uptake of $2.79 \pm 1.66\%$ ID/g, being higher than in all other organs and tissues apart from kidneys and blood at 2 h p.i. Receptor blocking studies revealed the observed tumor uptake to be solely mediated by integrin $\alpha_v\beta_3$, whereas no contribution of the GE11 peptide sequence to tumor uptake *via* the EGFR could be determined. Thus, the approach to develop radiolabeled EGFR- and integrin $\alpha_v\beta_3$ -bispecific HBPLs is in general feasible although another peptide lead structure than GE11 should be used as the basis for the EGFR-specific part of the agents.



INTRODUCTION

Common radiolabeled monospecific peptides are fully established in clinical routines for the detection, delineation, and characterization of human malignancies by means of positron emission tomography/computed tomography (PET/CT). However, the application of such compounds for receptor-specific tumor imaging can come to its limits if the corresponding tumor entity shows a high heterogeneity, which can also impact the target structures to be addressed by the radiopeptides. This can manifest in a very variable receptor expression, not only in terms of the intensity of expression but also in the form of the present receptor type. Moreover, the receptor expression can vary between and also within the same individual, not only affecting tumor imaging but also an efficient non-systemic tumor therapy, requiring the complete depiction of the full extent of the disease and thus its correct

staging.^{1–4} During disease progression^{5,6} or induced by therapy,^{7,8} the receptor expression status of lesions can also change, adding further complexity to this target expression issue. This can result in a limited tumor visualization sensitivity.

In contrast, the relatively new approach to combine two receptor-specific peptides into a heterobivalent peptidic ligand (HBPL), synergistically addressing two different molecular

Received: November 22, 2022

Accepted: December 15, 2022

Published: January 4, 2023



targets being overexpressed on the tumor entity can help to overcome the outlined problems.⁹ The most important characteristic is of course the ability of these constructs to be able to bind to two different receptor types, strongly increasing the tumor imaging probability due to the fact that the overall number of target receptors is increased and that a heterogeneous receptor expression profile does not pose a problem as long as at least *one* of the target receptors of the HBPL is present on the tumor cell (Figure 1).

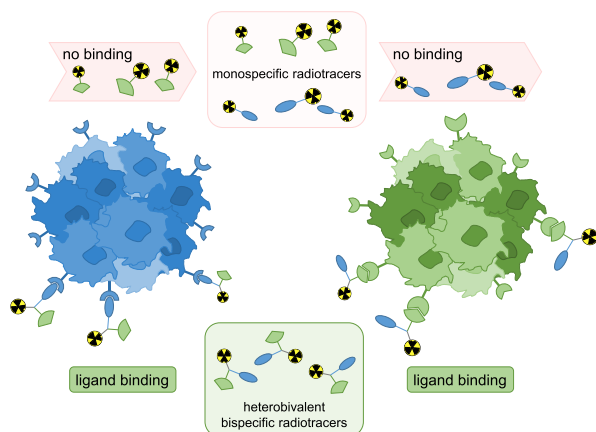


Figure 1. Schematic representation of the approach to utilize radiolabeled bispecific heterobivalent peptides for more sensitive imaging of tumors: whereas monospecific radiotracers are only able to interact with one receptor type and thus cannot bind any more if the target receptor expression is downregulated or completely missing (top), radiolabeled HBPLs exhibit a considerably higher tumor uptake probability due to their ability to address more than one receptor type (bottom), being still able to bind and thus visualize the tumor if at least *one* of the target receptors is present.

Another important point favoring bispecific binders over monospecific ones is their higher avidity (affinity of a bi- or multivalent binder) to the tumor—in case both target receptors are expressed concomitantly on the target cell. This does not even necessitate a high expression of both receptor types or the simultaneous binding of both peptide binders to both target receptors but is also achieved when one receptor type is expressed in a much lower density or if only one of the two peptides binds at a time. Moreover, radiolabeled HBPLs have a higher probability of rebinding upon dissociation from the receptor due to the so-called forced-proximity effect of the second peptide binder.

Due to these factors, radiolabeled HBPLs have been proposed to be very promising agents for the highly specific and sensitive visualization of tumors^{4,10} and have even found their way into clinical studies.^{11,12} There, they demonstrated the hypothesized higher tumor visualization sensitivities of breast cancer and prostate carcinomas, outperforming the corresponding monospecific radiotracers.

An interesting new combination of two peptides to a bispecific radiolabeled HBPL is based on agents targeting both the epidermal growth factor receptor (EGFR) and the integrin $\alpha_v\beta_3$. The EGFR—being also termed as human EGFR (HER1)—is part of the EGF receptor family, and its dysregulation is closely associated with oncogenesis and cancer progression. When upregulated, the EGFR is, for example, involved in tumor cell proliferation, angiogenesis, increased cell motility, induction of anti-apoptotic effects and metastatic

growth^{13–15} and is one of the most frequently altered oncogenes in solid cancer.¹⁶ As a result, EGFR overexpression is observed in many different cancer types, such as colorectal, lung, breast, prostate, head and neck, liver, ovary and esophageal cancer as well as gliomas and glioblastoma.^{16–19}

Integrin $\alpha_v\beta_3$, on the other hand, is closely associated with neoangiogenesis, tumor growth, as well as disease progression and metastasis,^{20–22} and its overexpression was observed in malignant melanoma, glioblastomas, breast, prostate, pancreatic, ovarian, and cervical cancer.²¹

Thus, the combination of two agents targeting both receptor types to one radiolabeled HBPL would result in a radiotracer being able to visualize a broad palette of tumor entities and in particular could enable a highly sensitive imaging of EGFR-overexpressing malignancies, showing a heterogeneous receptor expression profile. So far, only one example of such a hybrid agent has been described very recently.²³ The mentioned study dealt with the *in vitro* and *in vivo* evaluation of a ⁶⁸Ga-labeled HBPL being based on different building blocks: a GE11 peptide for EGFR targeting, a c(RGDyK) peptide for integrin $\alpha_v\beta_3$ -specific cell uptake, a NOTA (1,4,7-triazacyclononane-1,4,7-triacetic acid) chelator for ⁶⁸Ga-labeling, and a cysteine as central branching unit connecting the different building blocks. Although the agent was not able to show convincing results in terms of *in vivo* tumor delineation in NCI-H292 tumor-bearing xenograft mice, the obtained results at least seemed to point to a tumor uptake being mediated by both receptor types, providing a good basis for further structural optimizations.

For this purpose, we created two different EGFR- and $\alpha_v\beta_3$ -bispecific agents, carrying GE11 as the EGFR-specific peptide, c(RGDfK)/c(RGDyK) as $\alpha_v\beta_3$ -bispecific binders, (1,4,7-triazacyclononane-4,7-diyl)diacetic acid-1-glutaric acid (NODA-GA) as the chelator, a symmetrically branching building block, and linkers of different lengths. The developed agents were radiolabeled with ⁶⁸Ga³⁺, evaluated regarding their hydrophilicity/lipophilicity profile and their stability toward peptidase degradation in human serum. Further, we investigated their uptake into EGFR-positive A431 cells *in vitro* and determined their affinity to both target receptors by competitive displacement assays on A431- and $\alpha_v\beta_3$ -positive U87MG cells. Finally, we evaluated the pharmacokinetic properties of the most promising HBPL by *in vivo* PET/CT imaging in A431 tumor-bearing xenograft mice to assess its potential for the receptor-specific visualization of EGFR- and/or $\alpha_v\beta_3$ -expressing tumors.

MATERIALS AND METHODS

General. Chemicals, Radiochemicals, and Materials for *In Vitro* Assays. All chemicals were purchased from commercial sources in analytical grade quality and used without further purification unless otherwise stated. Fmoc- and side chain-protected amino acids and all resins, namely, Fmoc-Ile-Wang resin LL (loading 0.31–0.40 mmol/g), rink amide resin (loading 0.40–0.80 mmol/g), rink amide MBHA resin LL (loading 0.36 mmol/g), Fmoc-Asp(NovaSyn TGA)-OAll (0.18–0.21 mmol/g), H-Asp(^tBu)-2-chlorotrityl resin (loading 0.73 mmol/g), as well as benzotriazol-1-yloxytripyrrolidino-phosphonium hexafluorophosphate (PyBOP) were purchased from NovaBiochem (Darmstadt, Germany). Bis(2,5-dioxopyrrolidin-1-yl) 4,7,10,13,16,19-hexaoxadocosanedioate (PEG₅-bis-NHS ester) was purchased from BroadPharm (San Diego, USA), *tetrakis*(triphenylphosphine)palladium(0) (Pd-

(PPh₃)₄) from TCI (Eschborn, Germany), and 4-(4,7-bis(2-(*t*-butoxy)-2-oxoethyl)-1,4,7-triazacyclononan-1-yl)-5-(*tert*-butoxy)-5-oxo-pentanoic acid ((*R*)-NODA-GA(⁶Bu)₃) from CheMatech (Dijon, France). Bis-succinimidyl-4,7,10,13-tetraoxahexadecane-1,16-dioate (PEG₃-bis-NHS ester), 15-(9-fluorenylmethoxycarbonyl)amino-4,7,10,13-tetraoxapentadecanoic acid (PEG₃, Fmoc-NH-PEG₃-COOH), 21-(9-fluorenylmethoxycarbonyl)amino-4,7,10,13,16,19-hexaoxaheptacosanoic acid (PEG₅, Fmoc-NH-PEG₅-COOH), and 2-(bis(3-(((9*H*-fluoren-9-yl)methoxy)-carbonylamino)-propyl)-amino)-acetic acid potassium hemisulfate ((Fmoc-NH-Propyl)₂Gly-OH × KHSO₄) were obtained from Iris Biotech (Marktredwitz, Germany). Dichloromethane (DCM), diethylether, dimethylformamide (DMF), piperidine, 2-(1*H*-benzotriazol-1-yl)-1,1,3,3-tetramethyluronium hexafluorophosphate (HBTU), trifluoroacetic acid (TFA), and water were purchased from Carl Roth (Karlsruhe, Germany), acetonitrile (MeCN) from Häberle Labortechnik (Lonsee-Ettelschieß, Germany), and *N,N*-diisopropylethylamine (DIPEA), triisopropylsilane (TIS), and *L*-ascorbic acid from Sigma-Aldrich (Taufkirchen, Germany). Formic acid was obtained from Thermo Fisher Scientific (Schwerte, Germany). Human serum (pooled serum from male AB clotted whole blood) was also purchased from Sigma-Aldrich (Taufkirchen, Germany). A431 epidermoid carcinoma cells and U87MG human glioblastoma cells were obtained from DSMZ (Braunschweig, Germany) and ATCC (Wesel, Germany), respectively, and cell culture media from ATCC (Wesel, Germany) and Bio&SELL (Feucht, Germany). The recombinant human epidermal growth factor (hEGF) was obtained from Peprotech (Hamburg, Germany). [¹²⁵I]-EGF and [¹²⁵I]-eichistatin were both obtained in a molar activity of 81.4 TBq/mmol from PerkinElmer (Rodgau, Germany) as custom syntheses. [⁶⁸Ga]GaCl₃ for ⁶⁸Ga-radiolabeling reactions was obtained from an IGG100 ⁶⁸Ge/⁶⁸Ga-generator system (Eckert&Ziegler, Berlin, Germany). H₂O (Tracepur quality), hydrochloric acid (30%, Suprapur quality) and sodium hydroxide (30%, Suprapur quality) for radiolabeling reactions were purchased from Merck (Darmstadt, Germany).

Instrumentation. High-performance liquid chromatography (HPLC): for HPLC chromatography, a Dionex UltiMate 3000 system was used together with Chromeleon Software (Version 6.80). For analytical chromatography, a Chromolith performance (RP-18e, 100–4.6 mm, Merck, Germany) and for semipreparative analyses, Chromolith (RP-18e, 100–10 mm, Merck, Germany) columns were used, respectively. For radioanalytical chromatography, a Dionex UltiMate 3000 system equipped with a Raytest GABI Star radioactivity detector was used together with a Chromolith performance (RP-18e, 100–4.6 mm, Merck, Germany) column. All operations were performed with a flow rate of 4 mL/min using H₂O (supplemented with 0.1% TFA or formic acid) and MeCN (also supplemented with 0.1% TFA or formic acid) as solvents. MALDI-TOF-MS: matrix-assisted laser desorption/ionization (MALDI) time-of-flight mass spectra were obtained utilizing a Bruker Daltonics Microflex spectrometer, linear acquisition mode, positive ion source, and 200 shots per spot. α -Cyano-4-hydroxycinnamic acid (α -CS) or 2,5-dioxybenzoic acid (GS) were chosen as the matrix, and the dried-droplet method was used for sample preparation on a micro scout target (MSP 96 target polished steel BC, Bruker Daltonics, Germany). The data were recorded with flexControl Version 3.3 and analyzed with flexAnalysis Version 3.3 software. HR-

ESI-MS: For high-resolution electrospray ionization mass spectroscopy (HR-ESI-MS), a Thermo Finnigan LTQ FT Ultra Fourier Transform Ion Cyclotron Resonance (Dreieich, Germany) mass spectrometer was used. γ -Counter: γ -counting was performed using a 2480 Wizard gamma counter system from PerkinElmer. Ultrasonic bath: ultrasound-assisted peptide syntheses were performed in a Bandelin Sonorex Super RK 225 H ultrasonic bath (Berlin, Germany) with the temperature of the water being kept at ambient temperature.

Peptide Syntheses. Solid-phase peptide synthesis (SPPS) was performed according to standard Fmoc protocols²⁴ in standard syringes (5–20 mL, HSW, Tuttlingen, Germany) being equipped with 35 μ m porous high-density polyethylene frits (Reichelt Chemietechnik, Heidelberg, Germany). Two different methods were used for coupling, namely, mechanical agitation, where reactions were carried out in DMF for 60 min on a shaker at ambient temperature using 4 equiv of the respective amino acid and 3.9 equiv of HBTU as the coupling reagent with 4 equiv of DIPEA as the base, and ultrasound-assisted couplings, where reactions were carried out in DMF for 15 min in an ultrasonic bath at ambient temperature using 2 equiv of the respective amino acid and 1.9 equiv of HBTU as the coupling reagent with 2 equiv of DIPEA as the base. Fmoc-protecting groups were removed using 50% piperidine in DMF (v/v) (2 and 5 min). Cleavage from the resin and simultaneous removal of acid-labile protecting groups were usually performed with a mixture of TFA, TIS, and H₂O (v/v/v; 95/2.5/2.5) for 2–3 h at ambient temperature, followed by evaporation of the volatile materials. The residues were dissolved in 1:1 MeCN/H₂O + 0.1% TFA (v/v), purified by semipreparative HPLC and subsequently lyophilized. Mass spectra of **1**, **2** and **4–12** can be found in the [Supporting Information](#) (Figures S1–S11).

HBPL 1 (NODA-GA-PEG₃-GE11-PEG₃-c(RGDyK)) (1). To a solution of HBPL intermediate **1** (**11**) (1.95 mg, 0.72 μ mol) in DMF (100 μ L) were added c(RGDyK)-PEG₃-NHS ester (**5**) (1.0 equiv, 0.72 μ mol, 0.7 mg) and DIPEA (2.0 equiv, 1.43 μ mol, 0.24 μ L) and stirred for 2 h. The crude product was purified by semipreparative HPLC, and the product was obtained as a white solid after lyophilization. Gradient: 0–80% MeCN + 0.1% formic acid in 10 min (R_t = 5.19 min), yield: 33% (0.85 mg). MALDI-TOF-MS (m/z) using α -cyano-4-hydroxycinnamic acid as the matrix substance for [M + H]⁺ (calculated): 3596.11 (3596.80), [M + Na]⁺ (calculated): 3617.73 (3618.79), [M + K]⁺ (calculated): 3633.49 (3634.76). HR-ESI-MS [M + H]³⁺ (calculated): 1199.6063 (1099.6064), [M + 3H + Na]³⁺ (calculated): 1207.2641 (1207.2695).

HBPL 2 (NODA-GA-PEG₅-GE11-PEG₅-c(RGDfK)) (2). To a solution of the HBPL intermediate **2** (**12**) (4.1 mg, 1.5 μ mol) in absolute DMF (1 mL) were added DIPEA (10.6 equiv, 15.9 μ mol, 2.6 μ L) and c(RGDfK)-PEG₅-NHS ester (**7**) (2.0 equiv, 2.9 μ mol, 3.1 mg). The reaction progress was monitored by analytical HPLC and was found to be complete within 60 min/90 min (ultrasound-assisted/mechanical), whereafter the volatile materials were removed under reduced pressure. The crude product was purified by semipreparative HPLC, giving the product as a white solid after lyophilization. Gradient: 10–50% MeCN + 0.1% TFA in 8 min (R_t = 5.94 min), yield: 64% (3.6 mg)/48% (2.7 mg) (ultrasound-assisted/mechanical). MALDI-TOF-MS (m/z) using α -cyano-4-hydroxycinnamic acid as the matrix substance for [M + H]⁺ (calculated): 3759.43 (3756.91), [M + Na]⁺ (calculated): 3781.38 (3778.8966), [M + K]⁺ (calculated): 3797.66 (3794.87), [M

+ Na + K]⁺ (calculated): 3819.90 (3820.33). HR-ESI-MS (*m/z*) for [M + 3H]³⁺ (calculated): 1252.9791 (1252.9764), [M + 4H]⁴⁺ (calculated): 939.9860 (939.9841).

c(RGDyK) (4). The peptide c(RGDyK) (4) c(Arg-Gly-Asp-D-Tyr-Lys) was synthesized in two steps. First, the linear peptide sequence Arg-Gly-Asp-D-Tyr-Lys was synthesized on a highly acid-sensitive H-Asp(^tBu)-2-chlorotrityl resin (loading 0.73 mmol/g, 137 mg, 0.1 mmol) according to standard protocols. The fully side chain functionality-protected sequence was then cleaved from the resin using DCM + 1% TFA (incubation: 3 × 5 min, 1 × 15 min). The peptide-comprising solutions were combined, and the volatile materials were evaporated under reduced pressure. The residue was taken up in DMF (130 mL), followed by the addition of DIPEA (3.5 equiv, 0.35 mmol, 60 μL) before the mixture was cooled to 0 °C and diphenyl phosphoryl azide (DPPA, 1.25 equiv, 0.125 mmol, 27 μL) was added. The reaction was allowed to warm to ambient temperature and stirred for 2 days before the volatile materials were evaporated under reduced pressure. The obtained residue was incubated with TFA/TIS 97.5/2.5 (v/v) for 2.5 h before the crude product was precipitated by the addition of cold diethylether (50 mL). After washing the precipitate twice with diethylether and drying, the product was purified by semipreparative HPLC and obtained as a white solid after lyophilization. Gradient: 0–60% MeCN + 0.1% formic acid in 10 min (*R_t* = 2.86 min), yield: 45% (28.1 mg). MALDI-TOF-MS (*m/z*) using α-cyano-4-hydroxycinnamic acid as the matrix substance for [M + H]⁺ (calculated): 619.73 (620.32), [M + Na]⁺ (calculated): 641.74 (642.30), [M + K]⁺ (calculated): 657.67 (658.27).

c(RGDyK)-PEG₃-NHS Ester (5). To a solution of c(RGDyK) (4) (11.6 mg, 18.7 μmol) in DMF (70 mL) were added PEG₃-bis-NHS ester (4 equiv, 74.8 μmol, 36.5 mg) and triethylamine (1.08 equiv, 20.2 μmol, 2.8 μL). After 30 min, the volatile materials were evaporated under reduced pressure, and the crude product was purified by semipreparative HPLC, giving the product as a white solid after lyophilization. Gradient: 0–100% MeCN + 0.1% formic acid in 6 min (*R_t* = 3.31 min), yield: 85% (15.7 mg). MALDI-TOF-MS (*m/z*) using α-cyano-4-hydroxycinnamic acid as the matrix substance for [M + H]⁺ (calculated): 993.16 (993.45), [M + Na]⁺ (calculated): 1014.09 (1015.43).

c(RGDfK) (6). The peptide c(RGDfK) (6) c(Arg-Gly-Asp-D-Phe-Lys) was synthesized on a solid support according to standard protocols using a commercially available Fmoc-Asp(NovaSyn TGA)-OAll resin (loading 0.18–0.21 mmol/g, 18 μmol), HBTU as the coupling reagent, and standard N_α-Fmoc amino acids. After the removal of the OAll-protecting group using a mixture of Pd(PPh₃)₄ (0.25 equiv, 4.5 μmol, 5.2 mg) and phenylsilane (24 equiv, 0.45 mmol, 53.2 μL) in DCM for 3 × 30 min, the cyclization was performed on the resin by the addition of HBTU (1 equiv, 18 μmol, 6.8 mg) for 1 h/16 h (ultrasound-assisted/mechanical). The cleavage of the crude product from the solid support and the simultaneous removal of acid-labile protecting groups were performed with a mixture of TFA, TIS, and H₂O (95/2.5/2.5, v/v/v) for 3 h at ambient temperature, followed by the evaporation of the volatile materials. The crude product was purified by semipreparative HPLC, and the product was isolated as a white solid after lyophilization. Gradient: 0–40% MeCN + 0.1% TFA in 8 min (*R_t* = 4.02 min), yield: 64% (6.9 mg)/56% (6.1 mg) (ultrasound-assisted/mechanical). MALDI-TOF-MS (*m/z*) using α-cyano-4-hydroxycinnamic acid as the matrix substance

for [M + H]⁺ (calculated): 604.10 (604.32). HR-ESI-MS (*m/z*) for [M + H]⁺ (calculated): 604.3199 (604.3202).

c(RGDfK)-PEG₅-NHS Ester (7). To a solution of c(RGDfK) (6) (5.0 mg, 8.3 μmol) in absolute DMF (500 μL) were added PEG₅-bis-NHS ester (1.3 equiv, 10.4 μmol, 6.0 mg) and DIPEA (3.5 equiv, 29.0 μmol, 5 μL). The reaction progress was monitored by analytical HPLC and was found to be complete within 15 min/60 min (ultrasound-assisted/mechanical), whereafter the volatile materials were evaporated under reduced pressure, and the crude product was purified by semipreparative HPLC, giving the product as a white solid after lyophilization. Gradient: 10–40% MeCN + 0.1% TFA in 8 min (*R_t* = 5.74 min), yield: 43% (4.8 mg)/38% (4.2 mg) (ultrasound-assisted/mechanical). MALDI-TOF-MS (*m/z*) using α-cyano-4-hydroxycinnamic acid as the matrix substance for [M + H]⁺ (calculated): 1065.38 (1065.51). HR-ESI-MS (*m/z*) for [M + H]⁺ (calculated): 1065.5105 (1065.5099).

GE11-PEG₃-NHS Ester (8). GE11-PEG₃-NHS ester (8) (NHS-PEG₃-Tyr-His-Trp-Tyr-Gly-Tyr-Thr-Pro-Gln-Asn-Val-Ile) was completely assembled on a solid support using a commercially available preloaded Fmoc-Ile-Wang resin LL (loading 0.31 mmol/g, 300 mg, 93 μmol) by successive conjugation of the respective N_α-Fmoc amino acids using HBTU as the coupling agent and DIPEA as the base. The only exception was the PEG₃-bis-NHS ester building block (4 equiv, 372 μmol, 181.7 mg), which was conjugated without prior HBTU activation but under DIPEA assistance (4 equiv, 372 μmol, 63.6 μL) within 1 h. The product was cleaved from the solid support and deprotected using TFA/TIS/H₂O 95/2.5/2.5 (v/v/v) within 1 h before the volatile materials were evaporated under reduced pressure, and the crude product was purified using semipreparative HPLC. The product was obtained as a white solid after lyophilization. Gradient: 20–80% MeCN + 0.1% formic acid in 10 min (*R_t* = 3.56 min), yield: 17% (30.2 mg). MALDI-TOF-MS (*m/z*) using α-cyano-4-hydroxycinnamic acid as the matrix substance for [M + H]⁺ (calculated): 1913.00 (1913.86), [M + Na]⁺ (calculated): 1935.07 (1935.84), [M + K]⁺ (calculated): 1951.10 (1951.82).

GE11-PEG₅-NHS Ester (9). The GE11-PEG₅-NHS ester (9) (NHS-PEG₅-Tyr-His-Trp-Tyr-Gly-Tyr-Thr-Pro-Gln-Asn-Val-Ile) was synthesized on a solid support according to standard protocols using a commercially available Fmoc-Ile-Wang resin LL (loading 0.31–0.40 mmol/g, 32 μmol), HBTU as the coupling reagent, standard N_α-Fmoc amino acids, and the PEG₅-bis-NHS ester as agents. The conjugation of the PEG₅-bis-NHS ester (5 equiv, 0.16 mmol, 92 mg/8 equiv, 0.26 mmol, 147 mg) was performed without prior activation with HBTU but under DIPEA assistance (4 equiv, 0.13 mmol, 21.9 μL) for 1 h or 15 min using mechanical agitation or ultrasound-assistance, respectively. The cleavage of the crude product from the solid support and the simultaneous removal of acid-labile protecting groups were performed with a mixture of TFA, TIS, and H₂O (95/2.5/2.5, v/v/v) for 3 h at ambient temperature, followed by evaporation of the volatile materials. The crude product was purified by semipreparative HPLC and the product was isolated as a colorless solid after lyophilization. Gradient: 0–60% MeCN + 0.1% TFA in 8 min (*R_t* = 6.36 min), yield: 26% (16.5 mg)/46% (29.2 mg) (ultrasound-assisted/mechanical). MALDI-TOF-MS (*m/z*) using α-cyano-4-hydroxycinnamic acid as the matrix substance for [M + H]⁺ (calculated): 2001.91 (2001.92). HR-ESI-MS (*m/z*) for [M + 2H]²⁺ (calculated): 1001.4607 (1001.4595).

NODA-GA-Bis-amino Dendron (10). The NODA-GA-bis-amino-dendron (**10**) was synthesized according to standard solid phase-based synthesis methods by coupling Fmoc-Lys(Mtt)-OH and Fmoc-PEG₃-OH to a standard rink amide resin (loading 0.4–0.8 mmol/g, 26.6 μ mol). Using TFA in DCM (1/99, v/v), the Mtt-protecting group of the lysine was removed within 45–90 min, followed by threefold washing of the resin with first DCM and afterward DIPEA in DCM (9/1, v/v) and conjugation of (*R*)-NODA-GA(^tBu)₃ (excess: 2 equiv instead of 4, 53.2 μ mol, 28.9 mg) to the ϵ -amino functionality of the lysine utilizing PyBOP instead of HBTU (excess: 1.9 equiv instead of 3.9, 50.5 μ mol, 26.3 mg) as the coupling reagent and prolonged reaction times of 30 min/2.5 h (ultrasound-assisted/mechanical). Afterward, (Fmoc-NH-Propyl)₂Gly-OH \times KHSO₄ (4 equiv, 106.4 μ mol, 81.9 mg) was coupled applying standard conditions but prolonged reaction times of 30 min/2.5 h (ultrasound-assisted/mechanical) to the amino functionality of the PEG₃-linker. Cleavage from the resin and the simultaneous removal of the acid-labile ^tBu-protecting groups were performed using a mixture of TFA, TIS, and H₂O (95/2.5/2.5, v/v/v) for 3 h at ambient temperature, followed by the evaporation of the volatile materials. The resulting residue was purified by semipreparative HPLC and the product isolated as a colorless, hardening oil after lyophilization. Gradient: 0–40% MeCN + 0.1% TFA in 8 min (*R*_t = 4.13 min), yield: 78% (19.1 mg)/54% (13.2 mg) (ultrasound-assisted/mechanical). MALDI-TOF-MS (*m/z*) using α -cyano-4-hydroxycinnamic acid as the matrix substance for [M + H]⁺ (calculated): 921.52 (921.56). HR-ESI-MS (*m/z*) [M + H]⁺ (calculated): 921.5616 (921.5615), [M + 2H]²⁺ (calculated): 461.2843 (461.2844).

HBPL Intermediate 1 (NODA-GA-Mono-amino-PEG₃-GE11 Dendron (11)). In a nitrogen atmosphere, GE11-PEG₃-NHS ester (**8**) (0.2 equiv, 2.6 μ mol, 5.0 mg) and DIPEA (0.5 equiv, 6.5 μ mol, 1.2 μ L) were added to a solution of NODA-GA-bis-amino dendron (**10**) (13.0 μ mol, 12 mg) in absolute DMSO (0.5 mL) and stirred for 2 h at ambient temperature. The solvent was removed under reduced pressure, and the crude product was purified by semipreparative HPLC, giving the product as a colorless hardening oil after lyophilization. Gradient: 0–80% MeCN + 0.1% formic acid in 10 min (*R*_t = 5.01 min), yield: 27% (1.95 mg). MALDI-TOF-MS (*m/z*) using α -cyano-4-hydroxycinnamic acid as the matrix substance for [M + H]⁺ (calculated): 2718.99 (2719.39), [M + Na]⁺ (calculated): 2740.94 (2741.37), [M + K]⁺ (calculated): 2757.00 (2757.34).

HBPL Intermediate 2 (NODA-GA-Mono-amino-PEG₅-GE11 Dendron (12)). To a solution of the NODA-GA-bis-amino dendron (**10**) (8.7 μ mol, 10.0 mg) in absolute DMF (1 mL) were added DIPEA (4.0 equiv, 35.1 μ mol, 6 μ L) and GE11-PEG₃-NHS ester (**9**) (0.6 equiv, 5.0 μ mol, 10.0 mg). The reaction progress was monitored by analytical HPLC and was found to be complete within 30 min/90 min (ultrasound-assisted/mechanical), whereafter the volatile materials were evaporated under reduced pressure. The crude product was purified by semipreparative HPLC, giving the product as a colorless solid after lyophilization. Gradient: 20–40% MeCN + 0.1% TFA in 8 min (*R*_t = 4.03 min), yield: 39% (9.5 mg)/25% (6.1 mg) (ultrasound-assisted/mechanical). MALDI-TOF-MS (*m/z*) using α -cyano-4-hydroxycinnamic acid as the matrix substance for [M + H]⁺ (calculated): 2809.09 (2807.44), [M + Na]⁺ (calculated): 2830.88 (2829.42), [M + K]⁺ (calculated):

2846.69 (2845.39). HR-ESI-MS (*m/z*) [M + 3H]³⁺ (calculated): 936.4859 (936.4845).

⁶⁸Ga-Radiolabeling of 1 and 2. Radiolabeling for log_{D(7.4)} determination, serum stability tests, and *in vitro* cell uptake studies: For radiolabeling with ⁶⁸Ga³⁺, [⁶⁸Ga]GaCl₃ was obtained by fractionated elution of a commercial ⁶⁸Ge/⁶⁸Ga-generator system (IGG100 system Eckert & Ziegler) with 0.1 M hydrochloric acid (HCl). A solution of the HBPLs **1** and **2** (1–20 nmol) in H₂O (Tracepur quality, 5–20 μ L) was added to 90–260 MBq [⁶⁸Ga]GaCl₃ (0.5–1.2 mL), and the pH was adjusted to 3.5–4.0 by the addition of sodium acetate solution (1.25 M, 100–150 μ L). After 10 min of reaction at 45–50 °C, samples were analyzed by analytical radio-HPLC. The radiolabeled products were found to be \geq 96% pure and obtained in non-optimized molar activities of 36–88 GBq/ μ mol.

Preparation of [⁶⁸Ga]Ga-1 for animal experiments: the [⁶⁸Ga]GaCl₃ generator eluate was obtained as described before and added to 10 \pm 2 mg of ascorbic acid. The pH of the solution was adjusted to 3.6–3.8 by the addition of sodium acetate solution (1.25 M, 150–175 μ L), followed by the addition of a solution of **1** (20 nmol) in H₂O (Tracepur quality, 20 μ L). After 15 min of reaction, the pH of the solution was adjusted to 7.0–7.4 using HEPES buffer (2 M, pH 8, 450 μ L) and analyzed by analytical radio-HPLC. The product exhibited a radiochemical purity of \geq 96%.

Determination of log_{D(7.4)} Values for [⁶⁸Ga]Ga-1 and [⁶⁸Ga]Ga-2. The water_{pH7.4}/1-octanol partition coefficient (log_{D(7.4)}) of the developed radiotracers was determined by the addition of a solution of the respective radiolabeled peptide (5 μ L, 0.5–2 MBq) to a mixture of 1-octanol (800 μ L) and phosphate buffer (0.05 M, pH 7.4, 795 μ L). The mixtures were vigorously shaken for 5 min on a mechanical shaker and subsequently centrifuged at 13,000 rpm for 2 min to achieve complete phase separation. 125 μ L of each phase was taken, and the amount of radioactivity in each phase was determined by γ -counting. Experiments were performed thrice, each in triplicate.

Determination of the Stability of [⁶⁸Ga]Ga-1 and [⁶⁸Ga]Ga-2 in Human Serum. A sample of the respective radiolabeled peptide (125 μ L, 10–30 MBq, pH 7.4) was added to human serum (500 μ L), which was pre-warmed and kept at 37 °C during the course of the experiment. At defined time-points (*t* = 0, 15, 30, 45, 60, and 90 min), 75 μ L of the mixture was added to 75 μ L of ice-cold ethanol, further cooled on ice for 5 min, and centrifuged at 13,000 rpm for 90 s. The supernatant was collected, the activity of the supernatant and the precipitate measured, whereafter the supernatant was analyzed by radio-HPLC. Experiments were performed thrice for each radioligand.

Cell Culture. A431 epidermoid carcinoma cells were grown in Dulbecco's modified Eagle medium (DMEM), high glucose medium (Gibco), supplemented with 10% (v/v) fetal bovine serum and 1% (v/v) penicillin–streptomycin (10,000 U/mL) at 37 °C in a humidified CO₂ (5%) atmosphere and were split at >80% confluence. U87MG primary glioblastoma cells were grown in EMEM, supplemented with 10% (v/v) fetal bovine serum and 1% (v/v) penicillin–streptomycin (10,000 U/mL) (Gibco) at 37 °C in a humidified CO₂ (5%) atmosphere and were split at >80% confluence.

Internalization Studies. A431 cells (10⁶ per well) were seeded into 24-well cell culture multiwell plates (Cellstar) and incubated for 2 days at 37 °C in a humidified CO₂ (5%)

atmosphere. Immediately before the experiment, each well was washed twice with fresh internalization medium (DMEM, high glucose containing 1% fetal bovine serum), followed by the addition of internalization medium to a final volume of 1.35 mL per well. To half of the wells was added phosphate-buffered saline (PBS), containing 0.5% bovine serum albumin (BSA) (150 μ L), while to the other half was added a blocking solution of a 100-fold molar excess of hEGF (5 nM) in PBS, containing 0.5% BSA solution (150 μ L), followed by incubation at 37 °C for 10 min. Thereafter, a solution of the respective radiolabeled peptide (0.05 nM) in the internalization medium (8 μ L) was added to each well, and the plate was incubated at 37 °C for 30 min, 1, 2 or 3 h. Afterward, the medium was separated from the cells and each well was washed twice with 1 mL of ice-cold internalization medium, the washing solutions were added to the collected internalization medium (this combined solution represents the unbound fraction) and measured using a γ -counter. To determine the surface-bound fraction, each well was incubated twice for 5 min with ice-cold glycine-buffer (pH 2.8, 0.05 M, 1 mL), and the supernatants were collected and measured. The internalized fraction was determined by lysing the cells twice for 5 min with sodium hydroxide solution (2 M, 1 mL), collection, and measurement of the solutions. The amount of the radiotracer in each fraction was determined by γ -counting and referenced against a standard solution of the radiolabeled peptide (8 μ L). Each experiment was performed thrice.

Competitive Displacement Studies on A431 and U87MG Cells. *In vitro* binding affinities were acquired by competitive displacement experiments, each performed in triplicate. MultiScreen_{HTS}-BV, 1,2 μ m 96-well plates were incubated with a PBS/BSA (1%) solution (200 μ L per well) for 1 h before use. Each well was seeded with 10⁵ A431 or U87MG cells, suspended in Opti-MEM I (GlutaMAX I) (A431 cells) or EMEM containing 20 mM Tris, pH = 7.4, and supplemented with 150 mM NaCl, 2 mM CaCl₂, 1 mM MgCl₂, 1 mM MnCl₂, and 0.1% BSA (U87MG cells). The plate was incubated at 37 °C for 1 h with 0.25 kBq [¹²⁵I]-EGF or [¹²⁵I]-echistatin (25 μ L) in the presence of 11 increasing concentrations ranging from 10⁻⁸ to 10⁻³ M of the respective competitor (1 or 2, 25 μ L) or 5 \times 10⁻¹⁰ M to 10⁻⁶ M (hEGF)/10⁻⁸ M to 5 \times 10⁻⁵ M c(RGDfK) or c(RGDyK) with one well empty ensuring 100% binding of the radioligand. After the incubation, the filters were washed three times with cold PBS (1 \times 200 μ L, 2 \times 100 μ L) to remove unbound [¹²⁵I]-EGF or [¹²⁵I]-echistatin, collected, and measured in a γ -counter. The 50% inhibitory concentration (IC₅₀) values for each compound were obtained by nonlinear regression analysis using GraphPad Prism Software (v5.04). Each experiment was performed at least three times, each experiment being performed in triplicate.

In Vivo Experiments. All animal experiments were performed in compliance with the German animal protection laws and protocols of the local committee (Regierungspräsidium Karlsruhe, approval number: 35-9185.81/G-246/20). For the animal studies, 4–6-week-old female nude BALB/c-AnN-Foxn-1^{nu/nu}-Rj mice (Javier, Le Genest-Saint-Isle, France) with an average weight of 20 g were used. For the inoculation of the A431 tumor, 2 \times 10⁶ cells were injected subcutaneously into the right posterior flank under isoflurane anesthesia. The tumor size was regularly measured with a caliper, and the examination by PET/CT was performed between days 10 and 19 after inoculation when the tumor reached an approximate diameter of 0.5 cm. Each animal received 5.0 \pm 1.9 MBq of

[⁶⁸Ga]Ga-1, intravenously injected into a lateral tail vein. In case of blocking experiments, the animals received, in addition, either endogenous hEGF (100 μ g) or unmodified c(RGDyK) (200 μ g) for blocking of EGF receptors or integrin $\alpha_v\beta_3$. Five animals were studied per group. Dynamic PET images were acquired over 90 min p.i., and CT images were obtained within further 20 min with a triple-modality Bruker Albira II small-animal PET/CT/SPECT scanner (Karlsruhe, Germany). After the end of the diagnostic imaging, the animals were sacrificed at 120 min p.i. and all organs (tumor, blood, heart, lung, stomach, small intestine, colon, spleen, pancreas, liver, kidney, brain, bone, and muscle) were collected and measured with a γ -counter.

The dynamic PET images were reconstructed using the Albira Suite Reconstructor (Bruker) with an iterative dynamic reconstruction with 12 iterations using a 2D-maximum-likelihood expectation-maximization algorithm and a cubic image voxel size of 0.5 mm after scatter and decay correction. Data were divided into time frames from 1 to 10 min (10 \times 1 min, 10 \times 2 min, 6 \times 5 min and 3 \times 10 min) for the assessment of temporal changes in the regional tracer accumulation. The CT images were obtained at 45 kVp, with currents of 0.4 mA (high dose and good resolution). Acquisitions of 400 projections were taken and a 250 μ m isotropic voxel size image was reconstructed *via* filtered back projection. The reconstructed PET data were manually fused with the CT images using PMOD 3.8.0.7 and analyzed. Volumes of interest (VOIs) were defined for the quantification of tracer accumulation in heart, kidneys, tumor, and muscle. The results for each VOI were calculated as standardized uptake value (SUV) (kBq/cm³) averaged for each time frame.

RESULTS AND DISCUSSION

Synthesis of the EGFR- and $\alpha_v\beta_3$ -Bispecific Heterobivalent Agents 1 and 2. As mentioned above, only one combined radiotracer has been developed so far aiming to address the mentioned two target receptors EGFR and $\alpha_v\beta_3$, demonstrating in *in vivo* evaluations, suboptimal pharmacokinetic properties with an insufficient tumor delineation ability.²³ The obtained results however indicate that the observed tumor uptake was mediated by both receptor types; hence, the work provides a good basis for further optimization of the molecular design. For this purpose, we first replaced the central cysteine building block which was used for molecular branching and connection of the required structure elements (chelator and both peptide binders) by a symmetrically branching (NH₂-propyl)₂Gly-OH structure element. By this, a more homogeneous HBPL structure was obtained and the artificial and rather lipophilic thio-pyrrolidine-2,5-dione formed during the Michael Addition conjugation reaction was replaced by physiologically compatible hydrophilic acid-amide bonds. Moreover, the NOTA chelator was replaced by a NODAGA, efficiently producing highly stable ⁶⁸Ga-complexes under very mild radiolabeling conditions and leaving the N₃O₃-coordination sphere of the radiometal untouched due to its conjugation *via* the additional, non-coordinating carboxylic functionality.²⁵ Finally, we introduced PEG linkers of different lengths into the molecule, enabling a spatial distance of the peptide binders from each other and the chelator, which might facilitate positive peptide–receptor interaction.^{26,27} By using different PEG linker lengths, we aimed to determine if this parameter has any influence on the receptor-specific binding of the HBPLs. For EGFR- and integrin $\alpha_v\beta_3$ -specific receptor

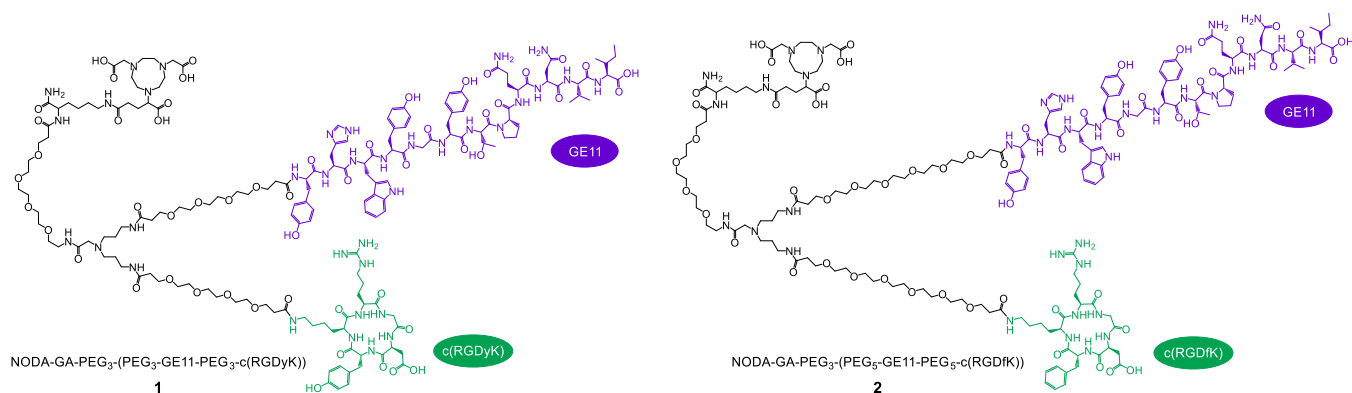


Figure 2. Structures of the HBPLs **1** and **2**. Both agents comprise a NODA-GA chelator being attached to the symmetrical branching unit *via* a PEG₃ linker. Whereas **1** comprises PEG₃ linkers for conjugation of the GE11 and c(RGDyK) peptides to the branching scaffold, PEG₅ linkers were introduced into **2** to enable a larger distance between the GE11 and c(RGDfK) peptide units.

targeting, the peptides GE11 and c(RGDyK)/c(RGDfK) were used as highly potent targeting units.^{15,28} In this context, GE11 has been shown to exhibit favorable EGFR targeting capabilities,¹⁵ whereas both integrin $\alpha_v\beta_3$ binders c(RGDyK) and c(RGDfK) are known to strongly interact with the target structure with high affinity²⁸ and should be studied in direct comparison to determine a potential influence of the respective peptide used on the *in vitro* parameters of the designed heterobivalent agents.

The structures of the developed HBPLs **1** and **2** are shown in Figure 2.

For the synthesis of **1** and **2**, a convergent synthesis approach was followed (Scheme 1): in the first step, the molecular building blocks **5** and **7–10** were synthesized and in two following steps reacted to give the final HBPLs **1** and **2**.

For the synthesis of c(RGDyK) (**4**) (Scheme 1A), the fully protected linear peptide intermediate **3** was built on a highly acid-sensitive solid support using standard Fmoc-based SPPS protocols.²⁴ Briefly, the carboxylic acid of the respective amino acid building block (applied in 4-fold excess) was usually activated for subsequent conjugation using HBTU (3.9-fold excess) and DIPEA (4-fold excess), generating the highly reactive active ester *in situ*, and the reaction was carried out for 30–60 min using mechanical agitation. After conjugation, the *N*-terminal Fmoc protecting group was removed by incubating the resin with piperidine/DMF 1/1 (v/v) for 2 and 5 min before the next amino acid was coupled.

After complete assembly of the amino acid sequence, the protected linear peptide intermediate **3** was cleaved from the solid support, cyclized in solution using DPPA and afterward deprotected to give the cyclic peptide sequence **4**. This was subsequently reacted with the PEG₃-bis-NHS ester to give the respective peptide NHS ester **5** (c(RGDyK)-PEG₃-NHS, Scheme 1A) required for acid-amine-based conjugation to the amino functionality-bearing symmetrically branched scaffold **10**.

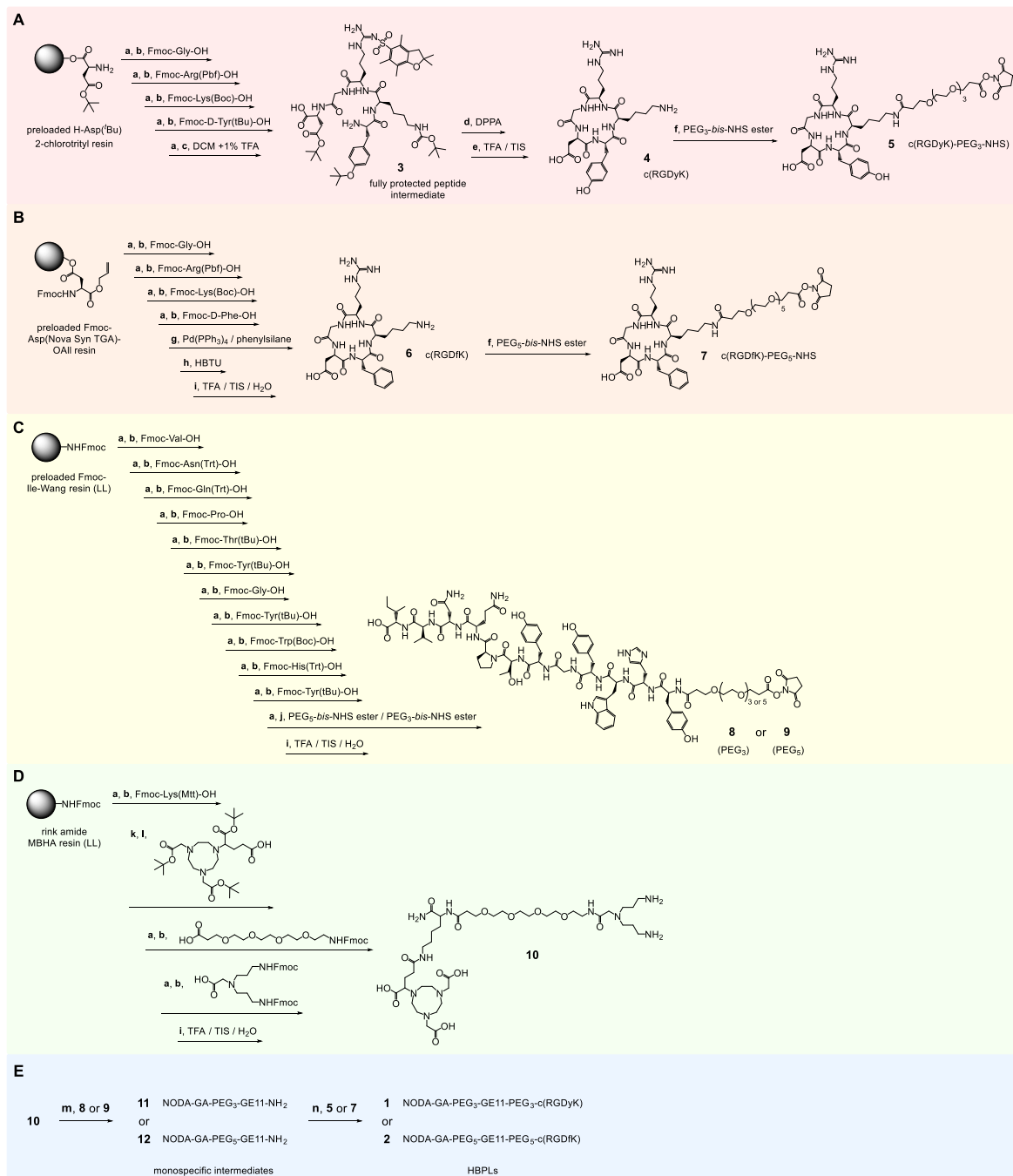
An alternative route for the preparation of cyclic peptides which was used for the synthesis of c(RGDfK) (**6**) is the complete assembly of the cyclized peptide on solid support (Scheme 1B). For this purpose, the first amino acid of the sequence, aspartic acid, is bound with its side chain functionality to the solid support, leaving the C-terminus and N-terminus free for assembly of the peptide sequence and its cyclization on resin. For **6**, the amino acid sequence was assembled as described before, using the same standard SPPS

protocols on a preloaded Fmoc-Asp(NovaSyn TGA)-O-allyl resin. In the following, the O-allyl-protecting group of the C-terminus was removed by incubation with Pd(PPh₃)₄ and phenylsilane before the peptide was cyclized on resin using 1 equiv of HBTU. The cyclic peptide was then cleaved from the resin and at the same time completely deprotected to give **6**, which was reacted in the next step in solution with PEG₅-bis-NHS ester to give **7** (c(RGDfK)-PEG₅-NHS, Scheme 1B).

The GE11 peptide derivatives comprising a PEG₃- or a PEG₅-NHS ester on the N-terminus (**8** and **9**, Scheme 1C) were synthesized accordingly on solid support by standard Fmoc-based SPPS. This included also the conjugation of the PEG₃-bis-NHS ester and PEG₅-bis-NHS ester, whereas the conjugation of the linkers in solution interestingly resulted in only negligible products yields due to the formation of a high number of unidentifiable side products, which prevented an efficient HPLC purification of the target peptide derivatives. The preparation of the symmetrically branched bis-amine **10** (Scheme 1D) was also performed completely on solid support, starting from a standard low-loading rink amide MBHA resin.

For the assembly of the different pre-synthesized building blocks to the target peptide heterodimers **1** and **2**, the branched bis-amine **10** was first reacted with the GE11-NHS ester **8** or **9** before the conjugation of the cyclic RGD peptide **5** or **7** took place (Scheme 1E). The reverse order of peptide conjugation, first introducing the RGD peptides and afterward the GE11 peptides, was tested first but was, contrary to the expectations, not successful. Following the reversed order of conjugation, it was anticipated that the conjugation of the large GE11 peptides, if carried out first, would prevent coupling of the second (much smaller) RGD peptides. However, the opposite effect was observed and the isolated monospecific cyclic RGD peptide intermediates could not be further reacted with the GE11 peptide NHS esters **8** and **9**, so that these had to be conjugated first to **10**, followed by the reaction with the RGD peptide NHS esters **5** and **7**. Another important factor influencing product yields during the conjugation reactions of **8** or **9** to **10**, giving the intermediates **11** and **12**, was the limited solubility of the bis-amino-dendron **10**, which can easily result in the sole formation of the GE11-homodimers despite large applied stoichiometric excesses of **10**. Thus, care has to be taken to ensure that **10** remains completely dissolved during the conjugation reaction in order to minimize the formation of the respective GE11 homodimer and favor

Scheme 1. Schematic Depiction of the Convergent Synthesis Strategy of the Bispecific Heterobivalent Peptidic Agents 1 and 2: (A) Synthesis of c(RGDyK)-PEG₃-NHS (5), (B) Synthesis of c(RGDfK)-PEG₅-NHS (7), (C) Synthesis of GE11-PEG₃/PEG₅-NHS (8/9), (D) Synthesis of Bis-Amino-Dendron (10), and (E) Synthesis of the Heterobivalent Agents 1 and 2 by Assembly of 10 with First 8/9 and Afterward with 5/7^a



^aReaction conditions: (a) cleavage of Fmoc-protecting group: piperidine/DMF (1/1, v/v), 2 + 5 min; (b) activation of amino acid: 4.0 equiv of amino acid derivative, 4.0 equiv of DIPEA, 3.9 equiv of HBTU in DMF, 2 min, 30–60 min; (c) mildly acidic cleavage from resin: DCM/TFA (99/1, v/v), 30 min; (d) cyclization of the peptide using DPPA: 1.25 equiv of DPPA, 3.5 equiv of DIPEA, DMF, 0 °C → ambient temperature, 2 days; (e) deprotection of side chain functional groups: TFA/TIS (95/5, v/v) for 2.5–3 h; (f) 4 equiv of PEG₃-bis-NHS ester, 1.08 equiv of TEA (triethylamine), DMF, 30 min; 1.3 equiv of PEG₅-bis-NHS ester, 3.5 equiv of DIPEA, DMF, 15 min; (g) *O*-allyl-deprotection: Pd(PPh₃)₄ (0.25 equiv), phenylsilane (24 equiv), DCM, 3 × 30 min; (h) cyclization: 1 equiv of HBTU in DMF, 1 h/16 h (ultrasound-assisted/mechanical); (i) cleavage of the peptide from the resin and simultaneous deprotection of side chain functional groups: TFA/TIS/H₂O (95/2.5/2.5, v/v) for 2.5–3 h; (j) 4 or 8 equiv of PEG_x-bis-NHS ester, 4 equiv of DIPEA, DMF, 1 h; (k) cleavage of Mtt-protecting group: 1% TFA in DCM, 3 × 15 min; (l) activation of (*R*)-NODA-GA(^tBu)₃: 2.0 equiv, 2.0 equiv of DIPEA, 1.9 equiv of PyBOP in DMF, 2 min, 30 min/2.5 h (ultrasound-assisted/mechanical); (m) 0.2 equiv of 8, 0.5 equiv of DIPEA, DMSO, 2 h; 0.6 equiv of 9, 4.0 equiv of DIPEA, DMF, 30 min/90 min (ultrasound-assisted/mechanical); (n) 1.0 equiv of 5, 2.0 equiv of DIPEA, DMF, 2 h; 2.0 equiv of 7, 10.6 equiv of DIPEA, DMF, 60 min/90 min (ultrasound-assisted/mechanical).

the formation of the intended products **11** and **12**. Following the outlined procedure, the target HBPLs **1** and **2** could be isolated in moderate to good yields over two steps of 9 and 25% for **1** and **2**, respectively.

Apart from the standard Fmoc-based SPPS and conjugation protocols, an alternative approach, being based on ultrasound-assistance instead of mechanical agitation was also tested during the syntheses of **2**, **6**, **7**, **9**, **10**, and **12**. Whereas the microwave-assisted peptide synthesis is an established way to increase the efficiency of SPPS,²⁹ the use of ultrasound for the same purpose is still a rather new approach.^{30–32} For the mentioned substances **2**, **6**, **7**, **9**, **10**, and **12**, both synthesis pathways were followed in parallel, each yielding the target product. However, the ultrasound-assisted conjugation reactions usually gave the products in higher yields while at the same time mostly requiring lower excesses of the activated building blocks and considerably shorter reaction times to complete the reactions (Table 1).

Table 1. Direct Comparison of the Applied Reaction Conditions and Obtained Results for the Syntheses of **2**, **6**, **7**, **9**, **10**, and **12**, Being Prepared Either Using Mechanical Agitation or Ultrasound-Assistance during the Individual Conjugation Reactions on Solid Support or in Solution

product	reaction pathway	reagent excess [equiv] ^a	required time for conjugation reactions [min] ^b	product yield [%]
2	mechanical	4	90	48 ± 2
	ultrasound	2	60	64 ± 8
6	mechanical	4	240 (+960 min cyclization)	56 ± 7
	ultrasound	2	60 (+60 min cyclization)	64 ± 7
7	mechanical	1.3	60	38 ± 8
	ultrasound	1.3	15	43 ± 8
9	mechanical	8	720	46 ± 12
	ultrasound	5	180	26 ± 7
10	mechanical	4	330	45 ± 3
	ultrasound	2	90	78 ± 6
12	mechanical	0.6	90	25 ± 7
	ultrasound	0.6	30	39 ± 2

^aExcess applied in each coupling reaction. ^bSummed over all relevant reaction steps.

The only exception from this trend was observed during the preparation of the GE11-PEG₅-NHS ester **9**, which was obtained in a lower yield of 26% using ultrasound-assistance, whereas it could be isolated in 46% yield using mechanical agitation. This can be attributed to the much higher reaction efficiency of ultrasound-assisted syntheses, which was however observed to be disadvantageous for the conjugation of the bis-PEG₅-NHS ester to the immobilized GE11 peptide on a solid support (Scheme 1C) as a result of the formation of a higher grade of crosslinks between two peptide units, being the most important side reaction in this synthesis step irrespective of the method used, mechanical or ultrasound-assisted synthesis.

Overall, both synthesis procedures gave the desired products **2**, **6**, **7**, **9**, **10**, and **12** in good yields but ultrasound-assistance can help to spare reagents, and more importantly, a considerable degree of time during the synthesis of peptidic compounds on the solid phase while giving the products in higher yields.

⁶⁸Ga-Radiolabeling of **1** and **2** and Evaluation of [⁶⁸Ga]Ga-1 and [⁶⁸Ga]Ga-2 with Regard to log_{D(7.4)} and Stability toward Human Serum Peptidase Degradation.

The obtained peptide heterodimers **1** and **2** were radiolabeled with ⁶⁸Ga using ⁶⁸Ga³⁺ being obtained as ⁶⁸GaCl₃ by the fractionated elution of a commercial ⁶⁸Ge/⁶⁸Ga-generator system. For this purpose, the pH of the generator eluate obtained as a 0.1 M HCl solution was adjusted to 3.5–4.0 by the addition of sodium acetate solution before 1–20 nmol of **1** or **2** was added and the reaction mixture was warmed to 45–50 °C for 10 min, yielding an almost quantitative incorporation of the ⁶⁸Ga of ≥96%. An equally efficient labeling with ⁶⁴Cu²⁺, yielding stable complexes as well, is possible under very similar conditions using a slightly different pH of 5.0 at ambient temperature.³³ The labeled agents [⁶⁸Ga]Ga-1 and [⁶⁸Ga]Ga-2 were obtained in radiochemical yields of ≥96% as well as non-optimized molar activities of 36 and 88 GBq/μmol, starting from 90 to 260 MBq ⁶⁸Ga³⁺ (Figure 3A, Table 2).

[⁶⁸Ga]Ga-1 and [⁶⁸Ga]Ga-2 were in the following evaluated with regard to their hydrophilicity/lipophilicity profile and their stability toward metabolic degradation by human serum peptidases. The hydrophilicity/lipophilicity profile of a radiotracer (being reflected in its log_{D(7.4)} value) is a good indicator for the likely major route of excretion during an *in vivo* application of the radiotracer.^{34,35} The log_{D(7.4)} values were determined by partition experiments of [⁶⁸Ga]Ga-1 and

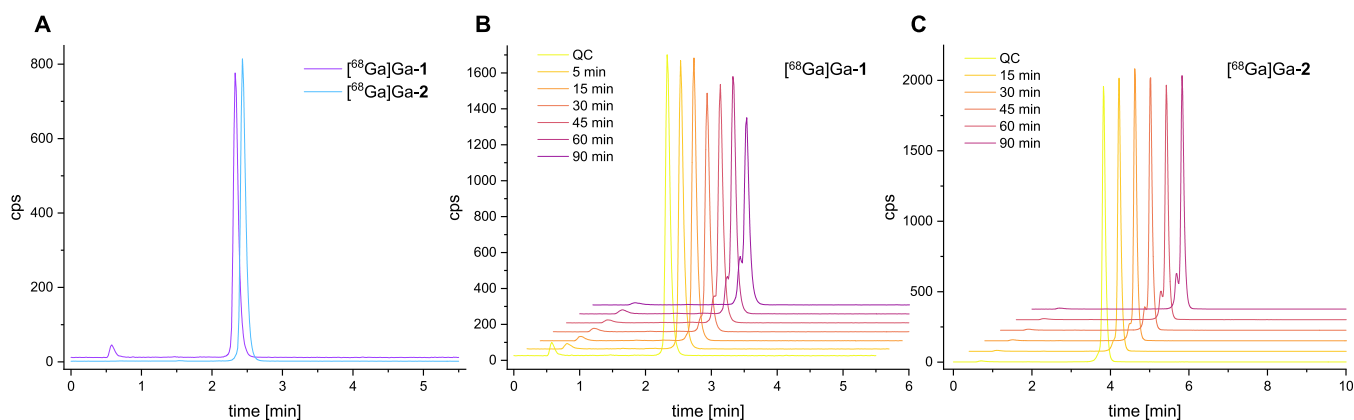


Figure 3. (A) Analytical quality control radio-HPLC chromatograms of [⁶⁸Ga]Ga-1 and [⁶⁸Ga]Ga-2; (B,C) depiction of the analytical radio-HPLC chromatograms obtained after incubation of [⁶⁸Ga]Ga-1 and [⁶⁸Ga]Ga-2 with pooled human serum at different time-points.

Table 2. Summary of the Chemical and Biological Properties of 1/[⁶⁸Ga]Ga-1 and 2/[⁶⁸Ga]Ga-2^a

	formula	calculated mass [<i>m/z</i>]	detected mass [<i>m/z</i>]	log _{D(7.4)}	A _m [GBq/μmol]	t _{1/2} in serum [min]	IC ₅₀
1/[⁶⁸ Ga]Ga-1	C ₁₆₆ H ₂₅₀ N ₃₆ O ₅₃	[M + H] ³⁺ : 1099.6064; [M + 3H + Na] ³⁺ : 1207.2695	[M + H] ³⁺ : 1099.6063; [M + 3H + Na] ³⁺ : 1207.2641	-3.07 ± 0.01	36	272	integrin α _v β ₃ : 1.39 ± 0.12 μM; EGFR: ND up to 25 μM
2/[⁶⁸ Ga]Ga-2	C ₁₇₄ H ₂₆₆ N ₃₆ O ₅₆	[M + 3H] ³⁺ : 1252.9764; [M + 4H] ⁴⁺ : 939.9841	[M + 3H] ³⁺ : 1252.9791; [M + 4H] ⁴⁺ : 939.9860	-3.44 ± 0.08	88	237	integrin α _v β ₃ : 1.48 ± 0.29 μM; EGFR: ND up to 1 mM

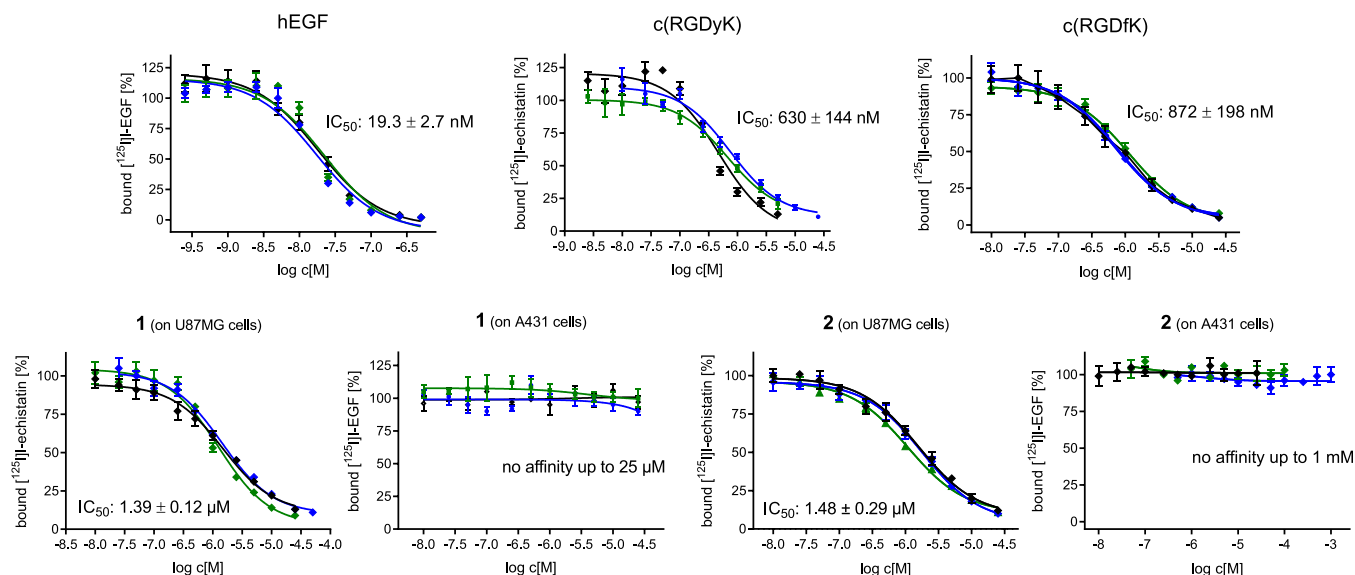
^aND: not determinable.

Figure 4. Graphical depiction of the results of the competitive displacements assays of hEGF, c(RGDyK), c(RGDfK), and both bispecific heterobivalent agents 1 and 2 on EGFR-positive A431 and integrin α_vβ₃-positive U87MG cells using [¹²⁵I]-EGF and [¹²⁵I]-echistatin as the competitors. Each experiment was performed thrice, each in triplicate.

[⁶⁸Ga]Ga-2 between an aqueous phosphate buffer phase at pH 7.4 and 1-octanol. For both agents, a similarly high hydrophilicity of -3.07 ± 0.01 and -3.44 ± 0.08 was determined for [⁶⁸Ga]Ga-1 and [⁶⁸Ga]Ga-2, respectively. The high hydrophilicity is desirable as the EGFR is—as outlined before—overexpressed on many different malignancies but EGFR-specific imaging is of special importance for the visualization of hepatocellular carcinomas (HCCs) and liver metastases of colon carcinomas.^{36,37} A relevant unspecific uptake of the heterobivalent radiotracers into the liver would hinder the sensitive detection of such lesions and is thus to be avoided.

Besides hydrophilicity/lipophilicity, also the stability of peptidic radiotracers against degradation is of relevance. The standard procedure to evaluate the susceptibility of the peptides toward degradation by peptidases is the determination of their stability in human serum. [⁶⁸Ga]Ga-1 and [⁶⁸Ga]Ga-2 were for this purpose incubated with commercially available pooled human serum of healthy donors at 37 °C. After defined time-points of 0, 15, 30, 45, 60, and 90 min, aliquots of the mixtures were taken and analyzed by analytical radio-HPLC (Figure 3B + C). The fraction of the intact radiopeptides was determined and the serum half-life of each radioligand was calculated, giving comparable values of 272 min for [⁶⁸Ga]Ga-1 and 237 min for [⁶⁸Ga]Ga-2. Thus, both heterobivalent radiotracers show a sufficient stability for application as ⁶⁸Ga-labeled PET imaging agents.

In Vitro Evaluation of the HBPLs Regarding Cell Uptake in A431 Cells and Receptor Affinity to Both Target Receptors—EGFR and Integrin α_vβ₃—On A431 and U87MG Cells. For both heterobivalent agents, the *in vitro* cell uptake into A431 cells (human epidermoid carcinoma cell line) was determined. A431 cells are the standard cell line for the evaluation of EGFR-specific radioligands^{38,39} as they are known to highly overexpress the EGFR.⁴⁰ Regarding the expression of integrin α_vβ₃, A431 cells are known to express this receptor type as well, although to an about 215-fold lower extent,⁴⁰ suggesting that a receptor-mediated uptake of [⁶⁸Ga]Ga-1 and [⁶⁸Ga]Ga-2 would mainly be driven by the EGFR. For the cell uptake studies, the cells were incubated with [⁶⁸Ga]Ga-1 and [⁶⁸Ga]Ga-2 in the absence and presence of the endogenous EGFR ligand hEGF to determine the EGFR receptor-specific cell interaction, and the results were differentiated by membrane-bound and internalized activity after 30 min and 1, 2, and 3 h. However, no EGF receptor-specific interaction was observed for both heterobivalent radiotracers. This absence of EGFR-specific cell interaction is at first sight surprising but is in line with other studies reporting similar results of a mainly unspecific interaction of GE11-based radioligands with tumor cell lines of different origins.^{41,42}

Thus, we, in the following, determined the *in vitro* binding affinity of both agents to both target receptors by competitive displacement assays on EGFR-positive A431 and integrin α_vβ₃-positive U87MG (human glioblastoma) cells. For this purpose, [¹²⁵I]-EGF and [¹²⁵I]-echistatin were used as competitors

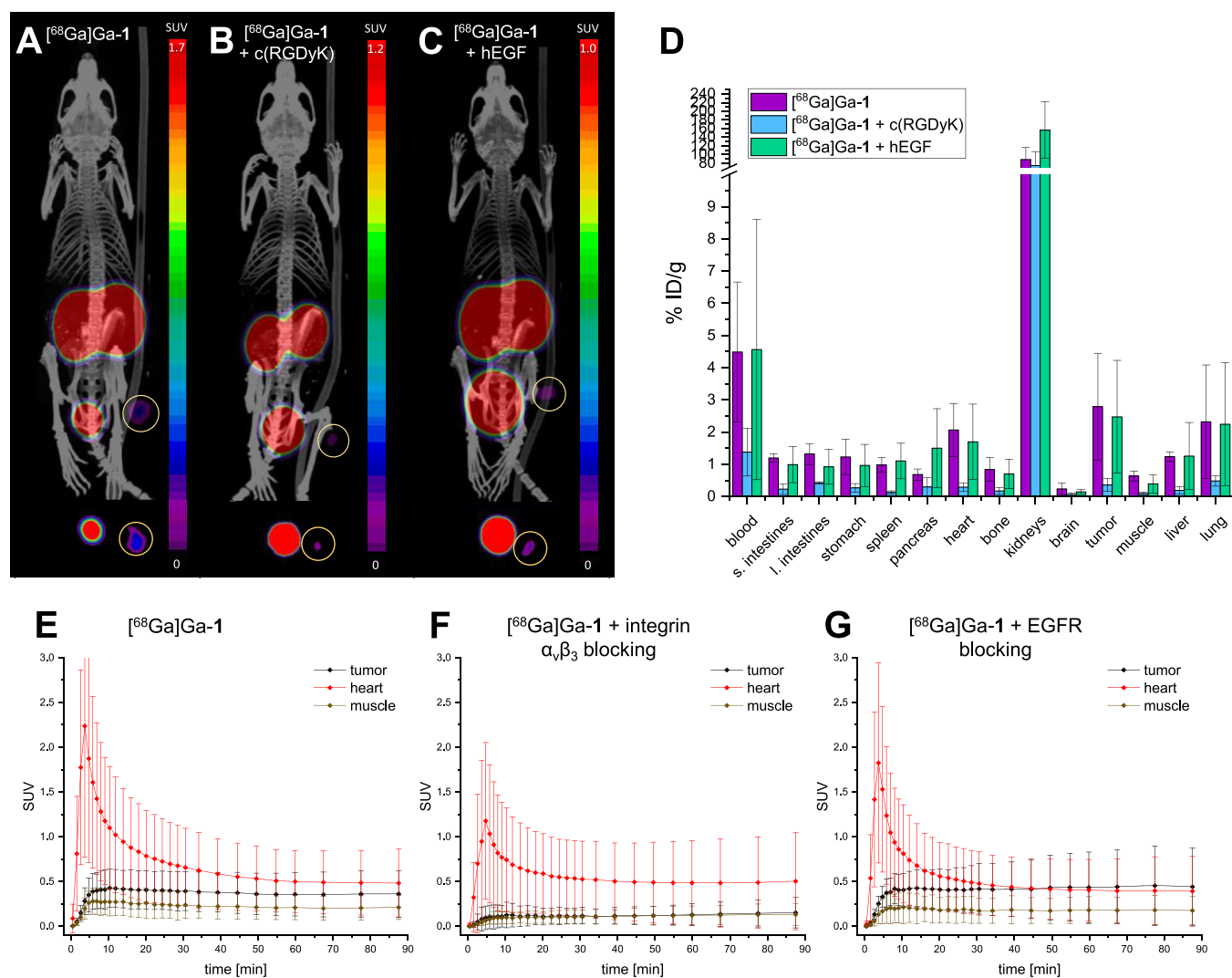


Figure 5. (A–C) Representative small animal PET/CT images for $[^{68}\text{Ga}]\text{Ga-1}$ without blocking (A), under integrin $\alpha_v\beta_3$ blockade using c(RGDyK) (B), and EGFR blockade using hEGF (C). The images show maximum intensity projections of the whole animals (upper panel) and transaxial slices at the tumor plane (lower panel) at 50–90 min p.i. Five animals were examined per group and the tumor is encircled in each image. (D) Results of the *ex vivo* biodistribution studies obtained at 120 min p.i. of $[^{68}\text{Ga}]\text{Ga-1}$ without blocking or under blockade of integrin $\alpha_v\beta_3$ or EGF receptors, expressed as % ID/g. Five animals were examined per group. (E–G) Time-activity curves—obtained from quantitative analysis of the PET/CT imaging data—for tumor, heart, and muscle of the animals without blocking (E), under integrin $\alpha_v\beta_3$ blocking (F), and EGFR blocking (G).

and hEGF, c(RGDyK) (4), and c(RGDfk) (6) were applied as internal references with known high affinity to their respective receptor types.^{28,43} The results of these assays are shown in Figure 4 (shown are the binding curves obtained for the reference compounds hEGF on A431 cells, c(RGDyK) and c(RGDfk) on U87MG cells and both HBPLs on U87MG and A431 cells).

The data show that the internal reference peptides hEGF, c(RGDyK), and c(RGDfk) showed the expected affinity to their respective targets with IC_{50} values of 19.3 ± 2.7 nM for hEGF to the EGFR, 630 ± 144 nM for c(RGDyK) and 872 ± 198 nM for c(RGDfk) to integrin $\alpha_v\beta_3$, being in the range of published values.^{44,45} In comparison, the HBPLs showed an only slightly decreased affinity to integrin $\alpha_v\beta_3$, presenting IC_{50} values to this receptor type of 1.39 ± 0.12 μM for 1 and 1.48 ± 0.29 μM for 2. In contrast, both heterobivalent agents failed to demonstrate any affinity toward the EGFR up to a concentration of 1 mM. This absence of EGFR-specific

receptor interaction of the HBPLs matches the results of the cell uptake studies. In order to find an explanation for this effect, we further determined the EGFR-specific affinity of unmodified GE11, being the lead for the developed HBPLs. Also, in this case, no EGFR-specific binding affinity could be found in the competitive displacement assays up to a concentration of 20 μM (data not shown). This is at first sight rather astonishing as GE11 was described to be a potent EGFR-specific agent.¹⁵ However, there is also a considerable number of publications that, like the present work, could not find any relevant affinity of GE11 to the EGFR.^{41,43,46,47} A theory recently proposed in this context—being based on the systematic investigation of the correlation between the valency of GE11 and the resulting EGFR affinities—is that GE11 shows relevant EGFR affinities only in the multivalent form but not as a monomer.⁴³

Nevertheless, we decided to investigate the pharmacokinetic profile of the most potent agent, $[^{68}\text{Ga}]\text{Ga-1}$, *in vivo* to

determine whether the *in vitro* results would be reproduced or whether the accessibility or addressability of the EGF receptor was improved under *in vivo* conditions, resulting in an $\alpha_v\beta_3$ - as well as EGFR-specific tumor uptake of the agent. By this, potential synergistic effects of peptide heterodimerization on the tumor uptake behavior or the biodistribution profile of the HBPL should be assessed.

In Vivo Evaluation of [^{68}Ga]Ga-1 in A431 Tumor-Carrying Xenograft Mice via PET/CT Imaging and Ex Vivo Biodistribution Experiments. For this purpose, we applied a standard A431 tumor xenograft mouse model to evaluate [^{68}Ga]Ga-1 regarding its pharmacokinetic profile and its applicability in PET imaging of EGFR- and/or $\alpha_v\beta_3$ -overexpressing tumors. We assumed that the tumor would—besides the EGFR—also express integrin $\alpha_v\beta_3$ to a considerable extent, enabling dual targeting via the heterobivalent bispecific radiotracer as under *in vivo* conditions and during tumor growth, the expression of integrin $\alpha_v\beta_3$ is usually upregulated. This can be attributed to the circumstance that tumors growing in size beyond 1–2 mm require the formation of a neovasculature to get access to sufficient amounts of oxygen and nutrients for further growth. This “angiogenic switch” is triggered by neoangiogenesis, being closely related to the expression of $\alpha_v\beta_3$ being thus upregulated in new formed tumor vessels.^{48,49}

To be able to determine the contribution of both peptidic binders to the total tumor uptake and to prove the specific interaction of the radioligand with both receptor types, blocking experiments were performed as well. In these, the uptake mediated by the EGFR or integrin $\alpha_v\beta_3$ was blocked by the co-administration of a 100-fold excess of either endogenous hEGF or unmodified c(RGDyK).

For the PET/CT imaging studies in the A431-bearing animals, 5.0 ± 1.9 MBq of [^{68}Ga]Ga-1 were administered via a lateral tail vein under isoflurane anesthesia, applying five animals per group. For the blocking experiments, the respective animals received the same amount of radiotracer together with hEGF or c(RGDyK). Directly after completion of the diagnostic scans at 120 min post injection (p.i.), the animals were sacrificed and the organs were collected and measured with a gamma-counter. The results of the *in vivo* and *ex vivo* experiments can be found in the form of PET/CT images, *ex vivo* biodistribution data, and time-activity curves (TACs) of selected organs obtained by quantitative analysis of the PET/CT data in Figure 5.

These data show that heterodimer [^{68}Ga]Ga-1 exhibited an accumulation in the tumor of $2.79 \pm 1.66\%$ ID/g at 2 h p.i., which was higher than in any other organ or tissue except from the kidneys ($88.04 \pm 28.51\%$ ID/g) and the blood ($4.49 \pm 2.17\%$ ID/g) at this time point. However, this nonetheless did not reflect in a very clear delineation of the tumor due to a relevant background accumulation of the agent, limiting the achievable contrasts. This can be attributed to the considerable residual activity in the blood of the animals of $4.49 \pm 2.17\%$ ID/g at 2 h p.i. The reason for this seems, however, not to be found in the slow pharmacokinetics of the compound (since the TACs clearly show that the accumulation in the tumor, muscle, and heart reached the plateau phase as early as 15 min p.i.) but rather in a non-specific interaction of the radioligand with serum proteins.

Regarding the receptor-specificity of the tumor uptake of [^{68}Ga]Ga-1, the blocking experiments revealed that the accumulation in the tumor seems to be solely mediated by

the integrin $\alpha_v\beta_3$, whereas the EGFR does not seem to contribute.

This is indicated, for example, by the data from the TACs (Figure 5E–G). These show for [^{68}Ga]Ga-1 a tumor uptake with an SUV of 0.43 ± 0.21 ($\text{SUV}_{\text{muscle}}: 0.27 \pm 0.16$), whereas under a c(RGDyK) blockade, the tumor uptake was reduced to the background level, resulting in comparable SUVs for tumor and muscle of 0.14 ± 0.13 and 0.13 ± 0.11 , respectively. In contrast, under an EGFR blockade, the $\text{SUV}_{\text{tumor}}$ remained unaltered with 0.45 ± 0.44 ($\text{SUV}_{\text{muscle}}: 0.18 \pm 0.16$).

These results were confirmed by the *ex vivo* biodistribution data (Figure 5D) showing that the absolute tumor uptake of [^{68}Ga]Ga-1 decreased by 87% in the case of integrin blockade applying an excess of c(RGDyK), which is also reflected in a visually considerably lower tumor accumulation in PET/CT (Figure 5A,B). Also, the uptakes in other organs such as liver, kidneys, lung, spleen, heart, intestines, and muscle decreased considerably, being in line with published data on the evaluation of the *in vivo* pharmacokinetics of radiolabeled RGD-peptide dimers in tumor-bearing mice.^{50,51}

In contrast, the tumor uptake of [^{68}Ga]Ga-1 did not decrease in the case of EGFR blocking, but even a higher tumor-to-muscle ratio was observed at 2 h p.i. under EGFR blockade compared to the experiments without receptor blocking. Also, the uptake of [^{68}Ga]Ga-1 into the liver and lungs, which express physiologically relevant amounts of EGFR,^{52,53} was not reduced by co-application of hEGF.

These results together demonstrate the existing integrin $\alpha_v\beta_3$ -specificity and the absence of EGFR-specificity of [^{68}Ga]Ga-1.

Since A431 cells by themselves show only a very low expression level of human integrin $\alpha_v\beta_3$ (vide supra), binding to murine $\alpha_v\beta_3$, which is expressed on activated endothelial cells during tumor angiogenesis, can be assumed here as mechanism being the basis for the observed tumor uptake. This can be attributed to the fact that human and murine $\alpha_v\beta_3$ show a very high homology of about 90%.⁵⁴ As a result, it has already been shown that c(RGDfK)-based compounds can bind to both human and murine $\alpha_v\beta_3$, confirming the assumption that the tumor uptake observed here is mediated by murine $\alpha_v\beta_3$.⁵⁵

In summary, we were able to demonstrate that it is feasible to design, synthesize, and radiolabel HBPLs based on integrin $\alpha_v\beta_3$ - and EGFR-specific peptide lead structures, efficiently producing radiolabeled hydrophilic and stable HBPLs. However, as indicated by the presented *in vitro* and *in vivo* results as well as by literature data, GE11 does not represent a suitable lead structure for achieving EGFR specificity. Thus, future attempts to develop integrin $\alpha_v\beta_3$ - and EGFR-bispecific radioligands should focus instead on other EGFR-specific peptides than GE11 to actually achieve the aimed bispecificity of the agents.

CONCLUSIONS

In the present study, we were able to show that it is feasible to design and synthesize radiolabeled heterobivalent agents based on integrin $\alpha_v\beta_3$ -specific cyclic RGD peptides and the putative EGFR-binder GE11. The agents, being assembled on a symmetrical, NODA-GA-modified and linker-comprising backbone via physiological acid-amide bonds, were efficiently labeled with $^{68}\text{Ga}^{3+}$ and showed high hydrophilicities and stabilities. The radiolabeled HBPLs demonstrated favorable integrin $\alpha_v\beta_3$ -specific receptor affinities but were in contrast

not able to receptor-specifically interact with the EGFR in *in vitro* studies. These *in vitro* results were confirmed by *in vivo* experiments in tumor-bearing mice, demonstrating the observed tumor uptake to be solely mediated by integrin $\alpha_v\beta_3$.

Based on the results obtained here, it can be concluded that the attempt to develop integrin $\alpha_v\beta_3$ - and EGFR-bispecific HBPLs is a promising approach, but the use of GE11 as a peptide lead to achieve an EGFR-specificity of the heterobivalent agents appears to be of limited utility for this purpose. Thus, future attempts to develop integrin $\alpha_v\beta_3$ - and EGFR-bispecific radioligands should focus instead on other EGFR-specific molecular scaffold than GE11 to achieve the aimed receptor-bispecificity for increased tumor visualization sensitivity and specificity.

■ ASSOCIATED CONTENT

SI Supporting Information

The Supporting Information is available free of charge at <https://pubs.acs.org/doi/10.1021/acsomega.2c07484>.

Mass spectra of **1**, **2**, and **4–12** and complete *ex vivo* biodistribution data of [⁶⁸Ga]Ga-**1** in A431 tumor-bearing mice (PDF)

■ AUTHOR INFORMATION

Corresponding Author

Carmen Wängler – Biomedical Chemistry, Clinic of Radiology and Nuclear Medicine, Medical Faculty Mannheim, Heidelberg University, 68167 Mannheim, Germany; orcid.org/0000-0003-1161-8669; Email: Carmen.Waengler@medma.uni-heidelberg.de

Authors

Diana Braun – Biomedical Chemistry, Clinic of Radiology and Nuclear Medicine, Medical Faculty Mannheim and Molecular Imaging and Radiochemistry, Clinic of Radiology and Nuclear Medicine, Medical Faculty Mannheim, Heidelberg University, 68167 Mannheim, Germany

Benedikt Judmann – Biomedical Chemistry, Clinic of Radiology and Nuclear Medicine, Medical Faculty Mannheim and Molecular Imaging and Radiochemistry, Clinic of Radiology and Nuclear Medicine, Medical Faculty Mannheim, Heidelberg University, 68167 Mannheim, Germany

Xia Cheng – Molecular Imaging and Radiochemistry, Clinic of Radiology and Nuclear Medicine, Medical Faculty Mannheim, Heidelberg University, 68167 Mannheim, Germany

Björn Wängler – Molecular Imaging and Radiochemistry, Clinic of Radiology and Nuclear Medicine, Medical Faculty Mannheim, Heidelberg University, 68167 Mannheim, Germany

Ralf Schirmmacher – Department of Oncology, Division of Oncological Imaging, University of Alberta, Edmonton, Alberta T6G 1Z2, Canada; orcid.org/0000-0002-7098-3036

Gert Fricker – Institute of Pharmacy and Molecular Biotechnology, University of Heidelberg, 69120 Heidelberg, Germany; orcid.org/0000-0003-3894-961X

Complete contact information is available at: <https://pubs.acs.org/10.1021/acsomega.2c07484>

Author Contributions

¹D.B. and B.J. contributed equally to this work.

Funding

This research project is part of the Forschungscampus M²OLIE and funded by the German Federal Ministry of Education and Research (BMBF) within the Framework “Research Campus—public-private partnership for Innovation” under the funding codes 13GW0389B and 13GW0388A.

Notes

The authors declare no competing financial interest.

■ ACKNOWLEDGMENTS

The authors thank Dr. Werner Spahl (LMU Munich) for performing the HR-ESI mass spectroscopy.

■ REFERENCES

- (1) Bedard, P. L.; Hansen, A. R.; Ratain, M. J.; Siu, L. L. Tumour heterogeneity in the clinic. *Nature* **2013**, *501*, 355–364.
- (2) Burrell, R. A.; McGranahan, N.; Bartek, J.; Swanton, C. The causes and consequences of genetic heterogeneity in cancer evolution. *Nature* **2013**, *501*, 338–345.
- (3) Reubi, J. C.; Fleischmann, A.; Waser, B.; Rehm, R. Concomitant vascular GRP-receptor and VEGF-receptor expression in human tumors: Molecular basis for dual targeting of tumoral vasculature. *Peptides* **2011**, *32*, 1457–1462.
- (4) Reubi, J. C.; Maecke, H. R. Approaches to Multireceptor Targeting: Hybrid Radioligands, Radioligand Cocktails, and Sequential Radioligand Applications. *J. Nucl. Med.* **2017**, *58*, 10s–16s.
- (5) Ananias, H. J. K.; van den Heuvel, M. C.; Helfrich, W.; de Jong, I. J. Expression of the Gastrin-Releasing Peptide Receptor, the Prostate Stem Cell Antigen and the Prostate-Specific Membrane Antigen in Lymph Node and Bone Metastases of Prostate Cancer. *Prostate* **2009**, *69*, 1101–1108.
- (6) Mannweiler, S.; Amersdorfer, P.; Trajanoski, S.; Terrett, J. A.; King, D.; Mehes, G. Heterogeneity of Prostate-Specific Membrane Antigen (PSMA) Expression in Prostate Carcinoma with Distant Metastasis. *Pathol. Oncol. Res.* **2009**, *15*, 167–172.
- (7) Diaz, L. A.; Williams, R. T.; Wu, J.; Kinde, I.; Hecht, J. R.; Berlin, J.; Allen, B.; Bozic, I.; Reiter, J. G.; Nowak, M. A.; Kinzler, K. W.; Oliner, K. S.; Vogelstein, B. The molecular evolution of acquired resistance to targeted EGFR blockade in colorectal cancers. *Nature* **2012**, *486*, 537–540.
- (8) Farag, S.; Smith, M. J.; Fotiadis, N.; Constantinidou, A.; Jones, R. L. Revolutions in treatment options in gastrointestinal stromal tumours (GISTs): the latest updates. *Curr. Treat. Options Oncol.* **2020**, *21*, 55.
- (9) Judmann, B.; Braun, D.; Wängler, B.; Schirmmacher, R.; Fricker, G.; Wängler, C. Current State of Radiolabeled Heterobivalent Peptidic Ligands in Tumor Imaging and Therapy. *Pharmaceuticals* **2020**, *13*, 173.
- (10) Fischer, G.; Schirmmacher, R.; Wängler, B.; Wängler, C. Radiolabeled heterobivalent peptidic ligands: an approach with high future potential for *in vivo* imaging and therapy of malignant diseases. *ChemMedChem* **2013**, *8*, 883–890.
- (11) Zhang, J.; Mao, F.; Niu, G.; Peng, L.; Lang, L.; Li, F.; Ying, H.; Wu, H.; Pan, B.; Zhu, Z.; Chen, X. 68Ga-BBN-RGD PET/CT for GRPR and Integrin $\alpha_v\beta_3$ Imaging in Patients with Breast Cancer. *Theranostics* **2018**, *8*, 1121–1130.
- (12) Zhang, J. J.; Niu, G.; Lang, L. X.; Li, F.; Fan, X. R.; Yan, X. F.; Yao, S. B.; Yan, W. G.; Huo, L.; Chen, L. B.; Li, Z. Y.; Zhu, Z. H.; Chen, X. Y. Clinical Translation of a Dual Integrin $\alpha_v\beta_3$ - and Gastrin-Releasing Peptide Receptor-Targeting PET Radiotracer, 68Ga-BBN-RGD. *J. Nucl. Med.* **2017**, *58*, 228–234.
- (13) Kaufman, N. E. M.; Dhingra, S.; Jois, S. D.; Vicente, M. D. H. Molecular Targeting of Epidermal Growth Factor Receptor (EGFR) and Vascular Endothelial Growth Factor Receptor (VEGFR). *Molecules* **2021**, *26*, 1076.

- (14) Rinne, S. S.; Orlova, A.; Tolmachev, V. PET and SPECT Imaging of the EGFR Family (RTK Class I) in Oncology. *Int. J. Mol. Sci.* **2021**, *22*, 3663.
- (15) Genta, I.; Chiesa, E.; Colzani, B.; Modena, T.; Conti, B.; Dorati, R. GE11 Peptide as an Active Targeting Agent in Antitumor Therapy: A Minireview. *Pharmaceutics* **2018**, *10*, 2.
- (16) Thomas, R.; Weihua, W. H. Rethink of EGFR in Cancer With Its Kinase Independent Function on Board. *Front. Oncol.* **2019**, *9*, 800.
- (17) Santarius, T.; Shipley, J.; Brewer, D.; Stratton, M. R.; Cooper, C. S. A census of amplified and overexpressed human cancer genes. *Nat. Rev. Cancer* **2010**, *10*, 59–64.
- (18) Sigismund, S.; Avanzato, D.; Lanzetti, L. Emerging functions of the EGFR in cancer. *Mol. Oncol.* **2018**, *12*, 3–20.
- (19) Yarden, Y.; Pines, G. The ERBB network: at last, cancer therapy meets systems biology. *Nat. Rev. Cancer* **2012**, *12*, 553–563.
- (20) Brooks, P. C.; Clark, R. A. F.; Cheresch, D. A. Requirement of Vascular Integrin $\alpha v \beta 3$ for Angiogenesis. *Science* **1994**, *264*, 569–571.
- (21) Desgrosellier, J. S.; Cheresch, D. A. Integrins in cancer: biological implications and therapeutic opportunities. *Nat. Rev. Cancer* **2010**, *10*, 9–22.
- (22) Niu, G.; Chen, X. Y. Why Integrin as a Primary Target for Imaging and Therapy. *Theranostics* **2011**, *1*, 30–47.
- (23) Chen, C. J.; Chan, C. H.; Lin, K. L.; Chen, J. H.; Tseng, C. H.; Wang, P. Y.; Chien, C. Y.; Yu, H. M.; Lin, W. J. ⁶⁸Ga-labelled NOTA-RGD-GE11 peptide for dual integrin and EGFR-targeted tumour imaging. *Nucl. Med. Biol.* **2019**, *68*–69, 22–30.
- (24) Wellings, D. A.; Atherton, E. Standard Fmoc protocols. *Methods Enzymol.* **1997**, *289*, 44–67.
- (25) Spang, P.; Herrmann, C.; Roesch, F. Bifunctional Gallium-68 Chelators: Past, Present, and Future. *Semin. Nucl. Med.* **2016**, *46*, 373–394.
- (26) Liu, Z. F.; Yan, Y. J.; Chin, F. T.; Wang, F.; Chen, X. Y. Dual Integrin and Gastrin-Releasing Peptide Receptor Targeted Tumor Imaging Using ¹⁸F-labeled PEGylated RGD-Bombesin Heterodimer ¹⁸F-FB-PEG3-Glu-RGD-BBN. *J. Med. Chem.* **2009**, *52*, 425–432.
- (27) Lindner, S.; Michler, C.; Wängler, B.; Bartenstein, P.; Fischer, G.; Schirmacher, R.; Wängler, C. PESIN Multimerization Improves Receptor Avidities and in Vivo Tumor Targeting Properties to GRPR-Overexpressing Tumors. *Bioconjugate Chem.* **2014**, *25*, 489–500.
- (28) Kapp, T. G.; Rechenmacher, F.; Neubauer, S.; Maltsev, O. V.; Cavalcanti-Adam, E. A.; Zarka, R.; Reuning, U.; Notni, J.; Wester, H. J.; Mas-Moruno, C.; Spatz, J.; Geiger, B.; Kessler, H. A Comprehensive Evaluation of the Activity and Selectivity Profile of Ligands for RGD-binding Integrins. *Sci. Rep.* **2017**, *7*, 39805.
- (29) Pedersen, S. L.; Tofteng, A. P.; Malik, L.; Jensen, K. J. Microwave heating in solid-phase peptide synthesis. *Chem. Soc. Rev.* **2012**, *41*, 1826–1844.
- (30) Raheem, S. J.; Schmidt, B. W.; Solomon, V. R.; Salih, A. K.; Price, E. W. Ultrasonic-Assisted Solid-Phase Peptide Synthesis of DOTA-TATE and DOTA-linker-TATE Derivatives as a Simple and Low-Cost Method for the Facile Synthesis of Chelator-Peptide Conjugates. *Bioconjugate Chem.* **2021**, *32*, 1204–1213.
- (31) Merlino, F.; Tomassi, S.; Yousif, A. M.; Messere, A.; Marinelli, L.; Grieco, P.; Novellino, E.; Cosconati, S.; Di Maro, S. Boosting Fmoc Solid-Phase Peptide Synthesis by Ultrasonication. *Org. Lett.* **2019**, *21*, 6378–6382.
- (32) Wolczański, G.; Plóciennik, H.; Lisowski, M.; Stefanowicz, P. A faster solid phase peptide synthesis method using ultrasonic agitation. *Tetrahedron Lett.* **2019**, *60*, 1814–1818.
- (33) Litau, S.; Seibold, U.; Vall-Sagarra, A.; Fricker, G.; Wängler, B.; Wängler, C. Comparative Assessment of Complex Stabilities of Radiocopper Chelating Agents by a Combination of Complex Challenge and in vivo Experiments. *ChemMedChem* **2015**, *10*, 1200–1208.
- (34) Garayoa, E. G.; Schweinsberg, C.; Maes, V.; Brans, L.; Blauenstein, P.; Tourwe, D. A.; Schibli, R.; Schubiger, P. A. Influence of the Molecular Charge on the Biodistribution of Bombesin Analogues Labeled with the [^{99m}Tc(CO)(3)]-Core. *Bioconjugate Chem.* **2008**, *19*, 2409–2416.
- (35) Glaser, M.; Morrison, M.; Solbakken, M.; Arukwe, J.; Karlsen, H.; Wiggen, U.; Champion, S.; Kindberg, G. M.; Cuthbertson, A. Radiosynthesis and biodistribution of cyclic RGD peptides conjugated with novel [¹⁸F]fluorinated aldehyde-containing prosthetic groups. *Bioconjugate Chem.* **2008**, *19*, 951–957.
- (36) Choi, K. J.; Baik, I. H.; Ye, S. K.; Lee, Y. H. Molecular Targeted Therapy for Hepatocellular Carcinoma: Present Status and Future Directions. *Biol. Pharm. Bull.* **2015**, *38*, 986–991.
- (37) Feng, Q. Y.; Wei, Y.; Chen, J. W.; Chang, W. J.; Ye, L. C.; Zhu, D. X.; Xu, J. M. Anti-EGFR and anti-VEGF agents: Important targeted therapies of colorectal liver metastases. *World J. Gastroenterol.* **2014**, *20*, 4263–4275.
- (38) Oroujeni, M.; Xu, T. Q.; Gagnon, K.; Rinne, S. S.; Weis, J.; Garousi, J.; Andersson, K. G.; Löfblom, J.; Orlova, A.; Tolmachev, V. The Use of a Non-Conventional Long-Lived Gallium Radioisotope ⁶⁶Ga Improves Imaging Contrast of EGFR Expression in Malignant Tumours Using DFO-ZEGFR:2377 Affibody Molecule. *Pharmaceutics* **2021**, *13*, 292.
- (39) Chang, A. J.; De Silva, R. A.; Lapi, S. E. Development and characterization of ⁸⁹Zr-labeled panitumumab for immuno-positron emission tomographic imaging of the epidermal growth factor receptor. *Mol. Imaging* **2013**, *12*, 17–27.
- (40) Benedetto, S.; Pulito, R.; Crich, S. G.; Tarone, G.; Aime, S.; Silengo, L.; Hamm, J. Quantification of the expression level of integrin receptor $\alpha v \beta 3$ in cell lines and MR imaging with antibody-coated iron oxide particles. *Magn. Reson. Med.* **2006**, *56*, 711–716.
- (41) Striese, F.; Sihver, W.; Gao, F.; Bergmann, R.; Walther, M.; Pietzsch, J.; Steinbach, J.; Pietzsch, H. J. Exploring pitfalls of ⁶⁴Cu-labeled EGFR-targeting peptide GE11 as a potential PET tracer. *Amino Acids* **2018**, *50*, 1415–1431.
- (42) Jiao, H. L.; Zhao, X. M.; Han, J. Y.; Zhang, J. M.; Wang, J. F. Synthesis of a novel ^{99m}Tc labeled GE11 peptide for EGFR SPECT imaging. *Int. J. Radiat. Biol.* **2020**, *96*, 1443–1451.
- (43) Abourbeh, G.; Shir, A.; Mishani, E.; Ogris, M.; Rödl, W.; Wagner, E.; Levitzki, A. PolyIC GE11 polyplex inhibits EGFR-overexpressing tumors. *IUBMB Life* **2012**, *64*, 324–330.
- (44) Liu, S. Radiolabeled Cyclic RGD Peptide Bioconjugates as Radiotracers Targeting Multiple Integrins. *Bioconjugate Chem.* **2015**, *26*, 1413–1438.
- (45) Cheng, X.; Hübner, R.; von Kiedrowski, V.; Fricker, G.; Schirmacher, R.; Wängler, C.; Wängler, B. Design, Synthesis, In Vitro and In Vivo Evaluation of Heterobivalent SiFAlin-Modified Peptidic Radioligands Targeting Both Integrin $\alpha v \beta 3$ and the MC1 Receptor-Suitable for the Specific Visualization of Melanomas? *Pharmaceutics* **2021**, *14*, 547.
- (46) Rahmanian, N.; Hosseinimehr, S. J.; Khalaj, A.; Noaparast, Z.; Abedi, S. M.; Sabzevari, O. ^{99m}Tc-radiolabeled GE11-modified peptide for ovarian tumor targeting. *Daru* **2017**, *25*, 13.
- (47) Rahmanian, N.; Hosseinimehr, S. J.; Khalaj, A.; Noaparast, Z.; Abedi, S. M.; Sabzevari, O. ^{99m}Tc labeled HYNIC-EDDA/tricine-GE11 peptide as a successful tumor targeting agent. *Med. Chem. Res.* **2018**, *27*, 890–902.
- (48) Liu, Z.; Wang, F.; Chen, X. Integrin $\alpha(v)\beta(3)$ -Targeted Cancer Therapy. *Drug Dev. Res.* **2008**, *69*, 329–339.
- (49) Max, R.; Gerritsen, R. R. C. M.; Nooijen, P. T. G. A.; Goodman, S. L.; Sutter, A.; Keilholz, U.; Ruitter, D. J.; De Waal, R. M. W. Immunohistochemical analysis of integrin $\alpha v \beta 3$ expression on tumor-associated vessels of human carcinomas. *Int. J. Cancer* **1997**, *71*, 320–324.
- (50) Oxboel, J.; Brandt-Larsen, M.; Schjoeth-Eskesen, C.; Myschetzky, R.; El-Ali, H. H.; Madsen, J.; Kjaer, A. Comparison of two new angiogenesis PET tracers ⁶⁸Ga-NODAGA-E[c(RGDyK)]₂ and ⁶⁴Cu-NODAGA-E[c(RGDyK)]₂; in vivo imaging studies in human xenograft tumors. *Nucl. Med. Biol.* **2014**, *41*, 259–267.
- (51) Zheng, Y. M.; Ji, S. D.; Tomaselli, E.; Yang, Y.; Liu, S. Comparison of biological properties of ¹¹¹In-labeled dimeric cyclic RGD peptides. *Nucl. Med. Biol.* **2015**, *42*, 137–145.

(52) Carver, R. S.; Stevenson, M. C.; Scheving, L. A.; Russell, W. E. Diverse expression of ErbB receptor proteins during rat liver development and regeneration. *Gastroenterology* **2002**, *123*, 2017–2027.

(53) Zhou, P.; Hu, J.; Wang, X. Q.; Wang, J. Y.; Zhang, Y.; Wang, C. Epidermal growth factor receptor expression affects proliferation and apoptosis in non-small cell lung cancer cells via the extracellular signal-regulated kinase/microRNA 200a signaling pathway. *Oncol. Lett.* **2018**, *15*, 5201–5207.

(54) Papo, N.; Silverman, A. P.; Lahti, J. L.; Cochran, J. R. Antagonistic VEGF variants engineered to simultaneously bind to and inhibit VEGFR2 and $\alpha v \beta 3$ integrin. *Proc. Natl. Acad. Sci. U.S.A.* **2011**, *108*, 14067–14072.

(55) Liu, Z.; Liu, S.; Niu, G.; Wang, F.; Liu, S.; Chen, X. Optical Imaging of Integrin $\alpha(v)\beta(3)$ Expression with Near-Infrared Fluorescent RGD Dimer with Tetra(ethylene glycol) Linkers. *Mol. Imaging* **2010**, *9*, 21–29.